# CITY OF PHOENIX COOL PAVEMENT PILOT PROGRAM

## PHASE II – 2022


### ASU Team

Ariane Middel, Jennifer Vanos, Kamil Kaloush, Jose Medina, David Sailor, Bill Campbell, Jolina Karam, Linus Napogbong, Portia Lartey, Mohammed Alhozaimy, Mansour Alhazmi, Zachary Van Tol, Gisel Guzman, student volunteers for fieldwork



October 2024

# Contents

## 1 Introduction

Intensifying summertime heat in Phoenix and many cities globally is a public and environmental health risk. Energy and water use, as well as the health of residents, are primary concerns during hot Phoenix summers—outcomes that are critical to quantify across various heat mitigation types. Often, cities of the Southwest are looked to as testbeds for urban resilience to the stresses of water resources, extreme heat, and population growth, and thus, critical assessments of interventions attempting to reduce these impacts are helpful to determine the value of more widespread implementation.

Various extreme heat interventions have been used across the Phoenix area. In 2020, the City of Phoenix initiated the Cool Pavement Pilot Program, applying CoolSeal by GuardTop® to 36 miles of residential streets in 8 neighborhoods. In partnership with researchers from Arizona State University (ASU), the City of Phoenix evaluated the performance of reflective Cool Pavement (CP) seal coat based on various metrics measured on the treated pavement as compared to the untreated areas (asphalt concrete) in the same residential neighborhood. Since 2020, the CoolSeal coating has been applied to streets in dozens of neighborhoods citywide. The City-University partnership continued into Phase II in 2022, building upon findings from Phase I. In the summer of 2022, the residential data collection continued to investigate further the impact of CP on various types of temperature, including the vertical air temperature gradient above the pavement (Section 2). Phase II also assessed CP impacts on water and energy use (Section 3) and human health (Section 4). A local testbed was established at the Union Hills Service Center facility in northern Phoenix to compare CP products of differing formulations (Section 5). Lastly, lab testing continued to investigate future CP impacts on RAP mixes, test surface durability, determine thermal properties of CP, and collect solar reflectance data (Section 6).

## 2 Residential Data Collection: Street-Level Air and Mean Radiant Temperature

In the summer of 2022, CoolSeal by GuardTop was applied across seven neighborhoods between May 31 and June 6, 2022. Phase II residential street data collection of Phoenix's CP Pilot Program was focused on quarter section Q15-13 in northwest Phoenix (Figure 1). This location is in the Maryvale neighborhood and contains relatively homogeneous characteristics with little outside influence from agricultural fields, industry, golf courses, or large parking lots. Within Q15-13 (coated during the week of May 31$^{st}$), the street-level data were collected between W Osborn Rd and W Thomas Rd to the north/south and N 67$^{th}$ Ave and N 63$^{rd}$ Ave to the west/east (Figure 1). The neighborhood's control ("traditional" asphalt) portion is east of the coated area between the same major roads to the north and south and between N 63$^{rd}$ Ave and N 61$^{st}$ Ave to the west/east. This portion of the neighborhood contains a somewhat worn chip-seal asphalt typical of many neighborhoods around the City. It is worth noting that conventional asphalt and sealant products are dark when first applied (solar reflectances typically around 5% to 8%), but reflectivity increases over time (perhaps to 10% to 15%). Further, CoolSeal is not an alternative to aged asphalt but rather an alternative to dark sealants. As such, the comparisons throughout this report reflect conservative estimates of the initial benefits of applying CoolSeal rather than a dark seal.

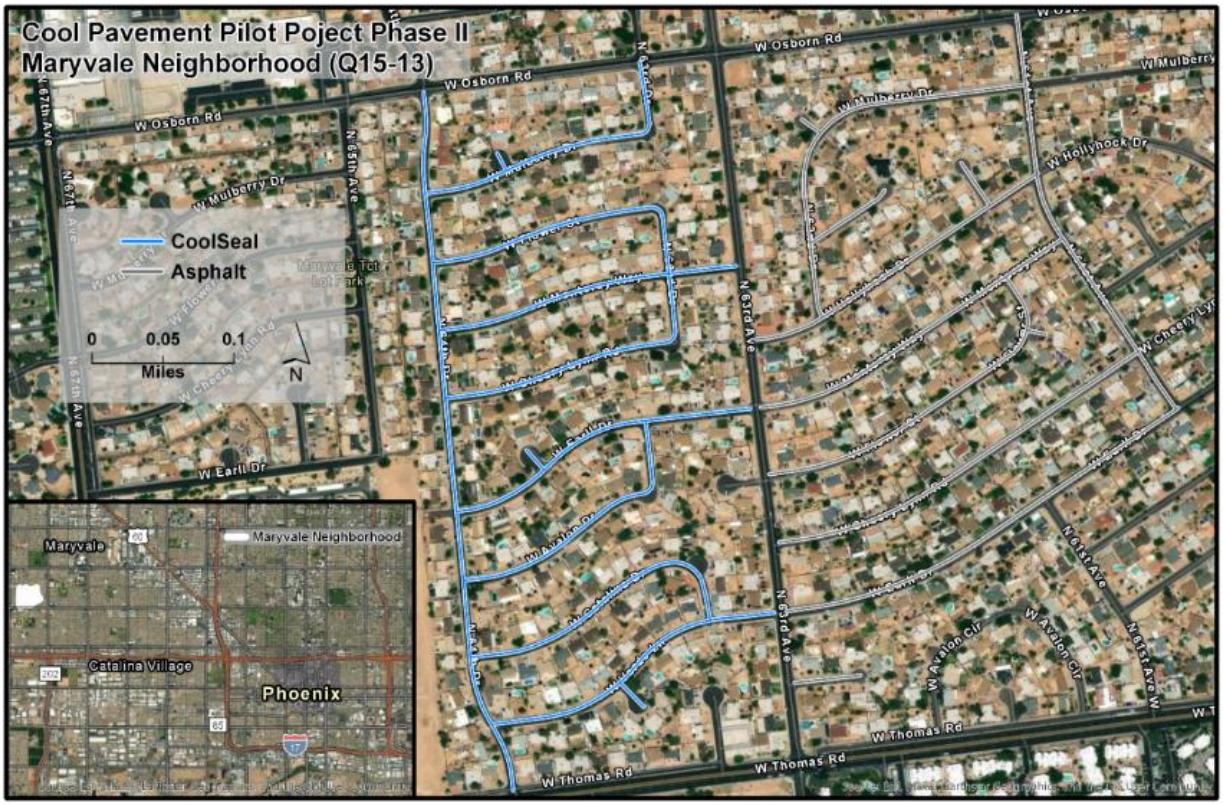


**Figure 1.** Q15-13, a northwest Phoenix neighborhood in Maryvale and the site of Phase II residential fieldwork efforts during the summer of 2022.

### Main Research Questions of the Field Study:

- How does the reflectance of different pavement coatings change over time?
- How does mean radiant temperature ($T_{MRT}$) compare pre- and post-coating at four times per day?
- How does air temperature ($T_{air}$) differ, on average, between coated and non-coated neighborhoods at four times per day? Does air temperature vary by height?

Data were collected in a pre/post fashion. Despite best efforts to conduct measurements on days with similar meteorological setups, the monsoon season made potential data collection days scarce throughout the summer. We attempted to have as similar weather as possible on the two test days, but differences in air temperature were present between May 26 and June 13, 2022. Both days were clear with low winds.

### 2.1 Mean Radiant Temperature Data Collection and Results

A mobile biometeorological cart (MaRTy) measured $T_{MRT}$, $T_{air}$, relative humidity, wind speed, and wind direction at pedestrian height at 2-second intervals. For comparison, $T_{MRT}$ was measured in both the CP-treated and untreated sections of Q15-13 before and after the CP application. Measurements occurred on May 26, 2022 (pre-coating) and June 13, 2022 (post-coating). Two MaRTy carts were used for these measurements: one stationary over the conventional asphalt (reference) located in the cul-de-sac of W Verde Ln (Figure 2a) and one mobile cart for transects over the experimental portion (pre-coating and post-coating) of the

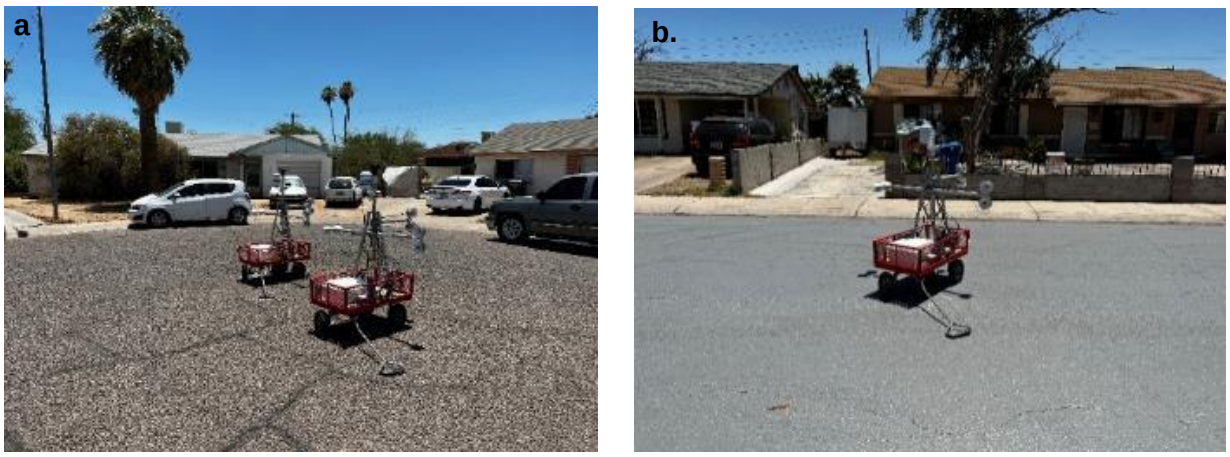


**Figure 2a.** MaRTy platforms at the comparison location (W Verde Ln) that remained untreated, and **b.** MaRTy at one of the transect locations over the CoolSeal on June 13, 2022.

neighborhood (Figure 2b). It should be noted that all MaRTy measurements were taken in the center of the road and are not representative of a pedestrian on an adjacent sidewalk. Transects occurred at four critical times of the day: pre-sunrise (~4:30 am), high sun (~12 pm), highest temperature (~4 pm), and post-sunset (7:30 pm). Data were collected at 11 locations above the CP to ensure spatial coverage of the neighborhood (Figure 3, yellow dots), with one outbound and one inbound transect (except for location 11), totaling 21 stops. This process allows averaging data across the hour to account for temporal changes and avoids the need for time detrending due to changes in weather within the hour.

Due to the difference in temperatures between the pre/post fieldwork days, particularly daily minimum temperatures, we do not report the pre-measurements in this report as they would be misleading. Table 1 shows same-day comparisons of the June 13th MaRTy transect stops over CP ($T_{MRT}^{CP}$) and measurements from the stationary MaRTy in the W Verde Ln cul de sac over regular asphalt ($T_{MRT}^{Asphalt}$). Same-day comparisons were calculated by subtracting the June 13th $T_{MRT}^{Asphalt}$ averages from the June 13th $T_{MRT}^{CP}$ measurements. Two stops that were shaded by a tree were excluded from the comparison.


**Figure 3:** Locations for data collection in the Maryvale neighborhood. Measurements were conducted on May 26, 2022, and June 13, 2022.

**Table 1.** The difference in average mean radiant temperature ($\Delta T_{MRT}$, °F) between asphalt and Cool Pavement (CP) in the Maryvale neighborhood by time of day. Measurements were taken before sunrise (~4:30–5:30 am), noon (12:00–1:00 pm), afternoon (4:00–5:00 pm), and post-sunset (~7:30-8:30 pm).

| | $\Delta T_{MRT}$ (°F) Before Sunrise | $\Delta T_{MRT}$ (°F) Noon | $\Delta T_{MRT}$ (°F) Afternoon | $\Delta T_{MRT}$ (°F) After Sunset |
|---|---|---|---|---|
| **Same-day comparison** (June 13, 2022) | | | | |
| $T_{MRT}^{CP} - T_{MRT}^{Asphalt}$ | -0.4 | +5.8 | +4.5 | -0.4 |

The difference between $T_{MRT}^{CP}$ and $T_{MRT}^{Asphalt}$ peaks during the middle of the day—with higher $T_{MRT}$ values above the CoolSeal relative to asphalt—as solar insolation reaches its maximum. During this day—June 13, 2022—the difference in $T_{MRT}$ peaked at 5.8°F around noon and dissipated to a 4.5°F difference during the afternoon transect before leveling post sunset. $T_{MRT}$ is relatively even between CP and asphalt pre-sunrise and after sunset.

### 2.2 Air Temperature Data Collection

We performed in-field, highly controlled, simultaneous tests of fine-scale $T_{air}$ variations by height (vertical gradient), using highly accurate resistance temperature detectors (RTD) while controlling for any potential localized effects of residential neighborhood design and land cover. Both stationary and mobile measurements were performed. A vertical RTD array with high-end, 3-wire RTDs was created to allow the array to be fastened to a bike for transects or connected to tripods for stationary measurements (Figure 4a,b). The 3-wire RTD sensors were procured from evosensors and have a range of -90ºF–500ºF with class A accuracy (accurate to ±0.2ºC). These sensors are designed for open-air applications and have a response time of 3 seconds during 3m/s airflow. All sensors were calibrated before data analysis. Sensors were fixed at four heights of interest (0.5m, 1.0m, 1.5m, and 2.0m) to create a temperature gradient above the surface. Measurements were logged continuously at 1-second intervals during each transect utilizing a Titan S8 Portable Data Acquisition Logger.

The array was utilized for stationary (partial diurnal profile) and mobile transect data collection. An effort was made to choose hot, clear days, but an emphasis was placed on calm winds to limit low-level mixing and reduce the external influence on temperature variations between the two surfaces. Monsoon weather in late summer 2022 made data collection particularly challenging. Data collection timing and conditions are provided in Table 2.

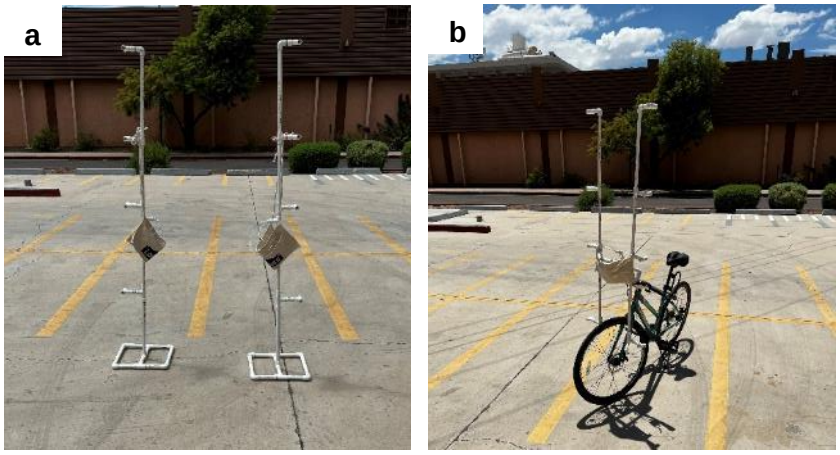


**Figure 4a.** RTD Temperature Array equipped to stands that allow for stationary temperature measurements at a 0.5m vertical gradient between 0.5m and 1m; **b.** RTD temperature array fixed to a bicycle that allows for mobile measurements.

**Table 2.** Dates of measurements using the RTD array. Stationary, continuous measurements were taken over the asphalt control area from 7:30 am–7:30 pm. Transect measurements moving over both CP and asphalt areas (see Figure 1) were taken within the following time windows: 12–1 pm, 1–2 pm, 4–5 pm, 5–6 pm, 8–9 pm, and 9–10 pm. The minimum, mean, and maximum daily air temperature ($T_{air}$) and maximum windspeed listed are from the National Weather Service weather station at Phoenix Sky Harbor.

| | Date | Min. Daily $T_{air}$ | Mean Daily $T_{air}$ | Max. Daily $T_{air}$ | Max Windspeed* |
|---|---|---|---|---|---|
| Transect | September 6th, 2022 | 87.0º F | 98.5º F | 110.0º F | 15mph |
| Stationary | October 21st, 2022 | 68.0º F | 79.0º F | 90.0º F | 13mph |

**Both days exhibited top wind speeds in the morning hours before a reduction in wind speed throughout the day.*

### *Mobile air temperature transect*

Bike transects were performed on September 6, 2022, at six hours of importance (12-1 pm and 1-2 pm for high sun, 4-5 pm and 5-6 pm for high temperature, and 7-8 pm and 8-9 pm for post-sunset temperature decay). Winds were relatively calm on this day, although a maximum gust of 15mph was measured around noon. Winds calmed significantly in the early evening.

The transect route was designed to cover approximately the same distance in the CoolSeal-coated and uncoated sections of the Q15-13 Maryvale neighborhood. A roughly 3-mile route was followed twice, in opposite directions, during the ~1hr transect to allow for a time-detrended average to be calculated for air temperatures above both neighborhood halves (Figure 5). Although difficult to maintain constant speed due to traffic, the bike was ridden at ~8mph on average to allow for ventilation of the sun-shielded sensors. Any stops/slow points of the transect were removed during the data cleaning process. $T_{MRT}$ values were then computed across each hour for each neighborhood portion at each height.

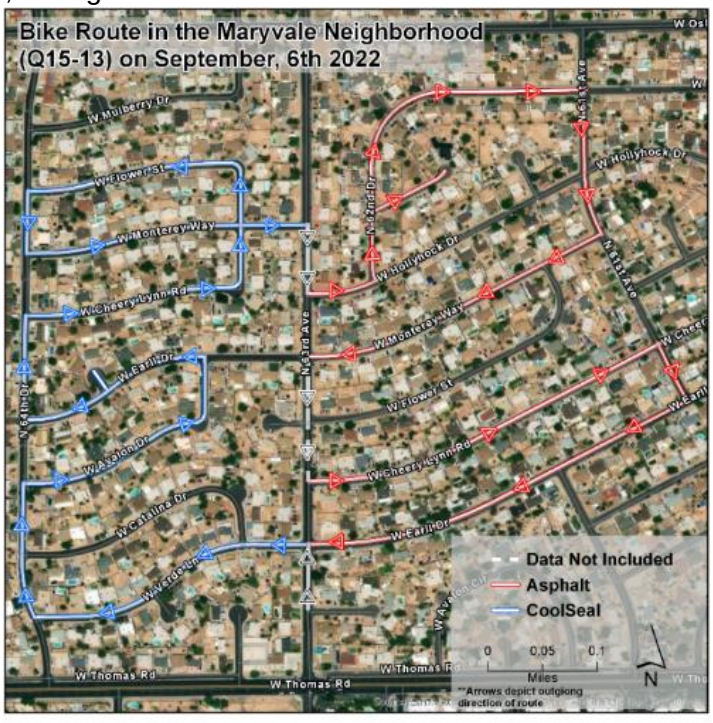


**Figure 5.** Map denoting the ~6mile round trip bike transect route followed 6 times over a 1 hour period per transect on September 6, 2022. Any portion of the transect on N 63rd Ave was not included in temperature calculations due to the higher likelihood of mixing between air above the two test areas (i.e., asphalt to east (red) and CP to west (blue)).

### *Stationary air temperature*

To increase the robustness of $T_{air}$ data and remove variability during the bike transects (e.g., varied speeds, traffic), stationary $T_{air}$ data collection occurred on October 21, 2022, continuously for 12 hours (7:30 am to 7:30 pm). Wind gusts reached a maximum of 13mph in the early morning before a calm, nearly breeze-less afternoon and evening.

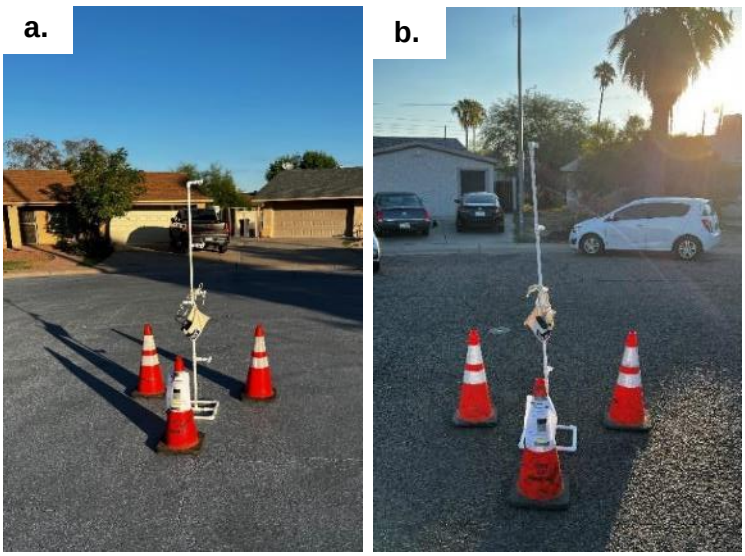


**Figure 6a.** Stationary RTD air temperature array over the CoolSeal in the cul de sac of W Earll Dr; and, **b.** the traditional asphalt in the cul de sack of W Verde Ln.

Two RTD temperature arrays (with four RTDs each at 0.5m, 1.0m, 1.5m, and 2.0m heights) were stationed in the center of two cul de sacs (one untreated conventional asphalt, one CP coated) in the Q15-13 neighborhood (Figure 6a, b). The arrays were ~0.3 miles apart. The untreated location was the W Verde Ln cul de sac to the southeast, and the CoolSeal location was the W Earll Dr cul de sac to the northwest (Figure 7). These locations were selected due to their similar geographic characteristics and low traffic. Measurements were logged continuously at 1-second intervals during the 12 hours of data collection utilizing Titan S8 Portable Data Acquisition Loggers.


**Figure 7.** Yellow diamonds indicate location of the RTD Temperature Arrays during stationary data collection on October 21, 2022 (W Eall Dr. and E Verde Ln).

## 2.3 Air Temperature Results

### *Mobile Transects*

The results from the bike transect on September 6 indicate that $T_{air}$ generally decreases with height as sensors are further from the influence of the underlying surface (Table App 1). Both test surfaces in the neighborhood reached a maximum recorded $T_{air}$ of nearly 111°F at 0.5m height during the 4 pm transect and a minimum recorded air temperature of around 97.5°F during the 9 pm transect. These trends are apparent in the bar plots of the transects at each respective height (Figure 8). Results show general consistency in $T_{air}$ values and by surface types across all transect times with a slight difference in magnitude.

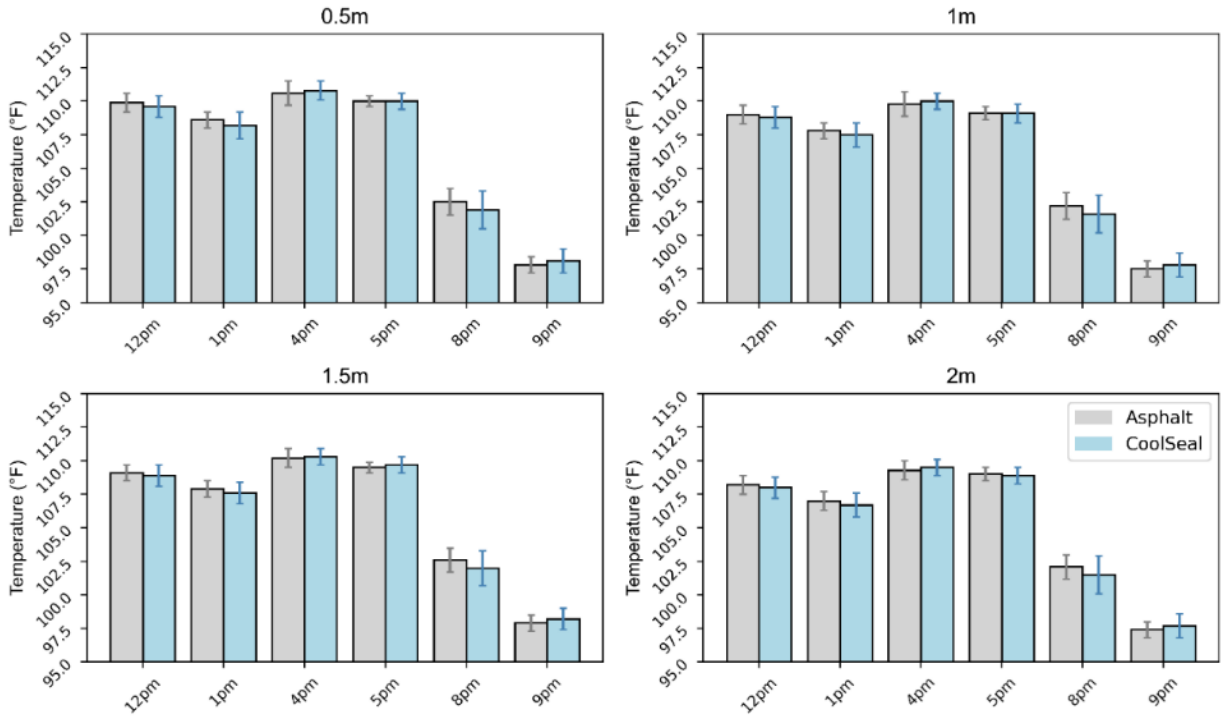


**Figure 8.** Bar charts of air temperature, with error bars, of each transect at each respective height for the CoolSeal and Asphalt portions of the Maryvale neighborhood on September 6, 2022.

Minor differences in mean $T_{air}$ values between the CoolSeal and traditional asphalt pavements are present (Table 3, Figure 9). Across all transects, at all heights, the $T_{air}$ difference is small. In most transect hours, $T_{air}$ is slightly lower over the Cool Seal portion of the neighborhood at all heights measured (an average difference of -0.13ºF across all heights and times measured). The starkest contrast is seen just after sunset (during the 8 pm transect) $T_{air}$ above CoolSeal was 0.6°F lower at all four heights relative to $T_{air}$ at corresponding heights above the asphalt. These values theoretically indicate the energy storage differences between the two materials as incoming insolation is no longer a factor, while radiative cooling of surfaces takes precedence. However, a reversal between $T_{air}$ differences above the two surfaces occurred between the 8 pm and 9 pm transects, where $T_{air}$ values increased above CoolSeal at all four heights during the transect. One potential explanation for this is the porous nature of the chip asphalt on the uncoated portion of the neighborhood relative to the much smoother half coated with CoolSeal.

The relative roughness of the asphalt surface induces a stronger influence of convective heat transfer as any sort of breeze blows over the neighborhood. Although seemingly minor, this influence could explain the difference in air temperature between 8 pm and 9 pm.

**Table 3.** The difference in mean air temperature ($T_{air}^{CP} - T_{air}^{Asphalt}$, °F) values over asphalt and Cool Pavement (CoolSeal) at four heights (0.5m, 1m, 1.5m, and 2m) on September 6, 2022, in the Maryvale neighborhood by time. One-hour bike transects were done midday (12 pm, 1 pm), afternoon (4 pm, 5 pm), and post-sunset (8 pm, 9 pm). Negative values on this table indicate cases where temperatures were lower over the CoolSeal surface, and positive values indicate instances where mean temperatures were lower over the asphalt portion of the neighborhood.

| Time | $\Delta T_{air}$ (°F) 0.5m | $\Delta T_{air}$ (°F) 1m | $\Delta T_{air}$ (°F) 1.5m | $\Delta T_{air}$ (°F) 2m |
|---|---|---|---|---|
| 12 pm | -0.4 | -0.3 | -0.3 | -0.3 |
| 1 pm | -0.3 | -0.2 | -0.2 | -0.2 |
| 4 pm | +0.2 | -0.2 | +0.1 | +0.2 |
| 5 pm | -- | -- | +0.2 | -0.1 |
| 8 pm | -0.6 | -0.6 | -0.6 | -0.6 |
| 9 pm | +0.3 | +0.3 | +0.3 | +0.3 |

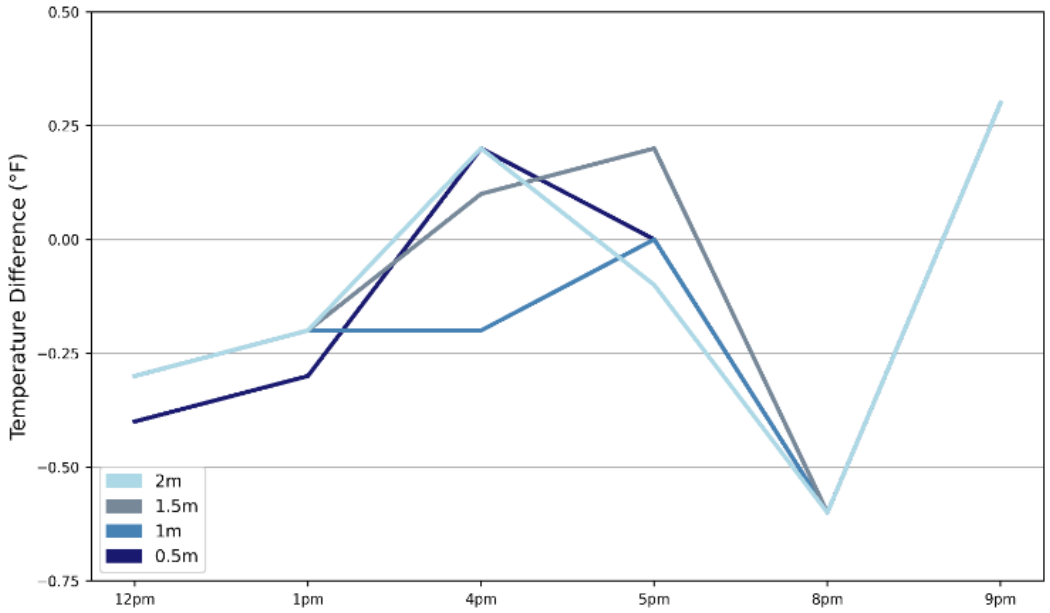


**Figure 9.** Visual depiction of the mean air temperature ($T_{air}^{CP} - T_{air}^{Asphalt}$, °F) difference above CoolSeal and asphalt at four heights during the six bicycle transects between 12 pm and 9 pm on September 6, 2022. Negative numbers on the graph indicate periods where the air temperature was higher over the asphalt, and positive number show times when the air temperature was higher over the CoolSeal product.

### *Stationary air temperature*

Results indicate similar temperature profiles at the four heights as found during the bike transects (Table App 2, Figure 10). However, the magnitude of temperature differences during the stationary setup is much larger than that of the bike transects in September (Table 6, Figure 11). Although the $T_{air}$ differences by height are larger in the stationary setup, comparisons between the two locations generally agree with mobile transects, showing slight temperature

decreases over the CoolSeal (an average difference of -0.9ºF across all heights and times measured) throughout the day, yet a similar reversal of this signal post sunset (Figure 11). However, the observed pattern of the stationary data is less conclusive across the four heights.

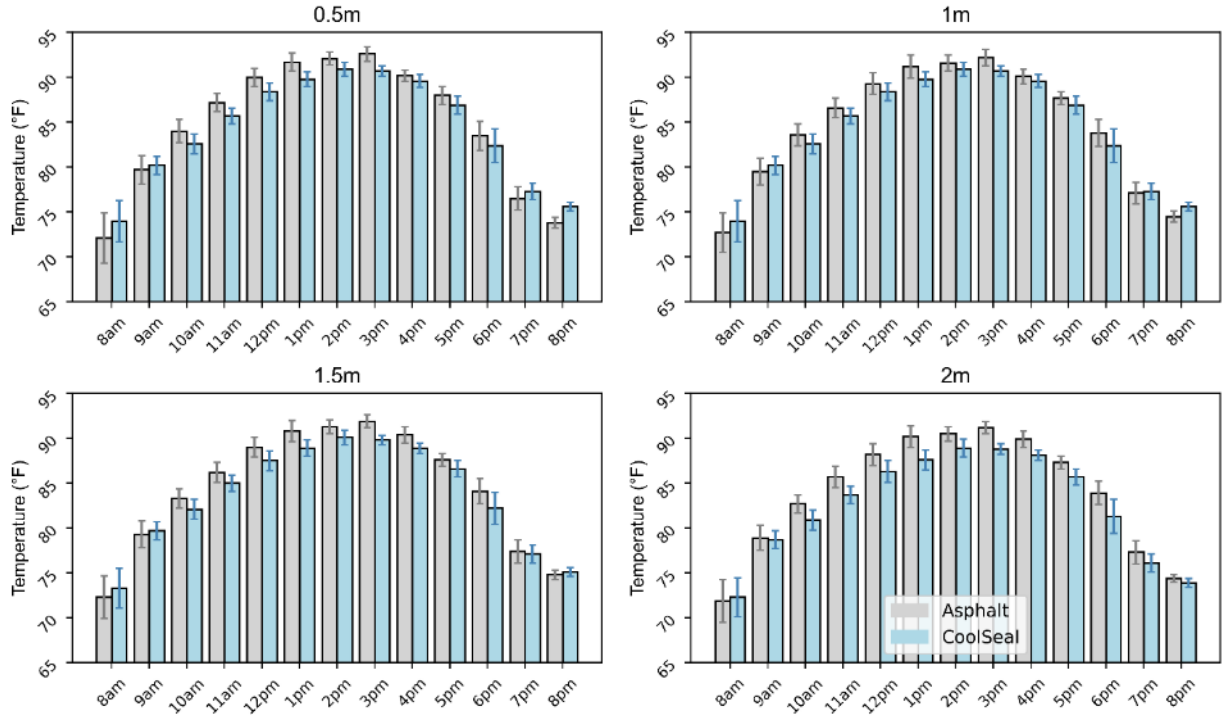


**Figure 10.** Bar charts of air temperature, with error bars, at each respective height for the CoolSeal and Asphalt portions of the Maryvale neighborhood on October 21, 2022.

**Table 6.** The difference in mean air temperature ($T_{air}^{CP} - T_{air}^{Asphalt}$, **°**F) values over asphalt and Cool Pavement (CoolSeal) at four different heights (0.5m, 1m, 1.5m, and 2m) in stationary spots on October 21, 2022, in the Maryvale neighborhood between ~7:30 am and ~8:30 pm.

| Time | $\Delta T_{air}$ (°F) 0.5m | $\Delta T_{air}$ (°F) 1m | $\Delta T_{air}$ (°F) 1.5m | $\Delta T_{air}$ (°F) 2m |
|---|---|---|---|---|
| 8 am | +1.9 | +1.3 | +1.0 | +0.4 |
| 9 am | +0.5 | +0.7 | +0.4 | -0.2 |
| 10 am | -1.4 | -1.0 | -1.2 | -1.8 |
| 11 am | -1.5 | -0.9 | -1.2 | -2.0 |
| 12 pm | -1.6 | -0.9 | -1.5 | -1.9 |
| 1 pm | -1.9 | -1.4 | -1.9 | -2.6 |
| 2 pm | -1.2 | -0.7 | -1.2 | -1.6 |
| 3 pm | -1.9 | -1.5 | -2.1 | -2.4 |
| 4 pm | -0.6 | -0.5 | -1.5 | -1.8 |
| 5 pm | -1.1 | -0.8 | -1.0 | -1.6 |
| 6 pm | -1.1 | -1.4 | -1.9 | -2.6 |
| 7 pm | +0.8 | +0.2 | -0.3 | -1.2 |
| 8 pm | +1.8 | +1.1 | +0.3 | -0.5 |

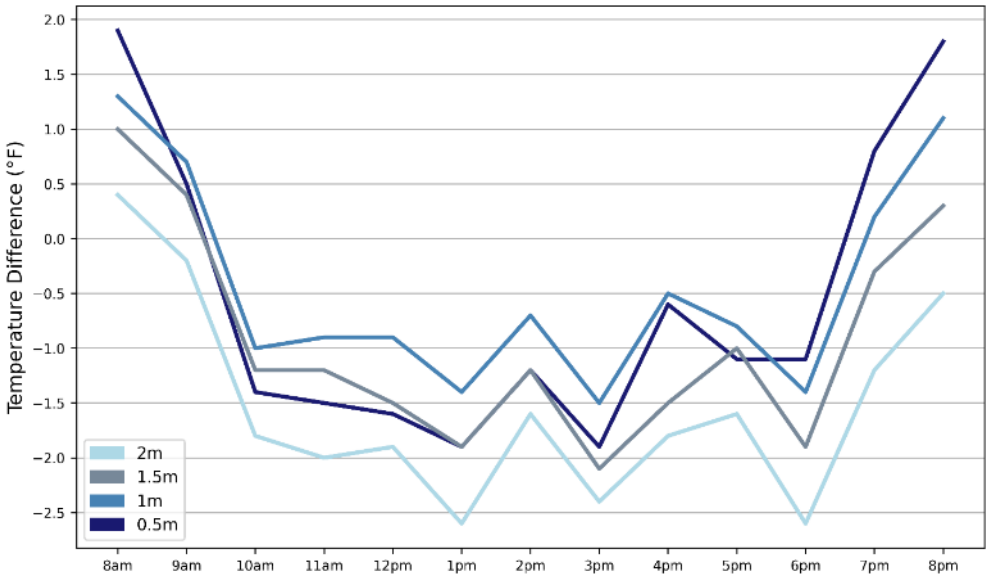


**Figure 11.** Visual depiction of the mean air temperature ($T_{air}^{CP} - T_{air}^{Asphalt}$, °F) difference above CoolSeal and asphalt at four different heights during a continuous 13 hours on October 21, 2022. Negative numbers on the graph indicate periods where the air temperature was higher over the asphalt, and positive number show times when the air temperature was higher over the CoolSeal product.

## 3 The impact of air temperature on water consumption and air conditioning

The main objective of this task is to understand the potential impact of CP on residential water use and energy consumption. We conducted a literature review for the sensitivity of residential water use to air temperature, focusing on previous studies in Phoenix. To assess the impact of CP on energy consumption, we explored the literature for energy use sensitivity to air temperature and conducted residential building energy simulations in EnergyPlus using the meteorological observations from field measurements in Section 2.

### 3.1 Water Savings

We have identified five sources from the peer-reviewed literature discussing the impact of an increase/decrease in $T_{air}$ on residential water use. These sources primarily focus on Phoenix as a hot, dry climate case study.

Using two databases, the first paper [1] investigates annual water use from 1980 to 2004. The first database derives annual average liters per capita per day (LPCD) delivered by the City's water services department to the City's customers on a per capita basis. The second database records monthly data for single-family residential properties from 1995 to 2004, with records being the sum of all users, then divided by the total number of users. The mean annual water use per household in Phoenix is estimated to be 911.3 liters (240.74 gallons) per capita per day. The results show that for every 1.0°C (1.8°F) increase (decrease) in air temperature, the detrended per capita residential water use increases (decreases) by 60.76 liters (16.05 gallons) per capita per day, representing a sensitivity of 6.7%/°C (or 3.7%/°F).

Two other studies by Guhathakurta et al. [2,3] focus primarily on residential water consumption in Phoenix in June. The data gathered from these related studies were derived from Water Services Department data sets. The average water consumption for June is 17,000 gallons/household, or 567 gallons/day per household. The results from [2] show that increasing daily minimum temperatures by 0.63 °C (1°F) is associated with an average monthly increase in water use of 290 gallons for a typical single-family unit, representing a sensitivity of 2.7%/°C (or 1.5 %/°F). The second study [3] estimated that increasing the daily diurnal temperature range by 1°F leads to an increase of 379 gallons in average water demand in single-family units for June, representing a sensitivity of 3.5%/°C (or 1.9%/°F)**.**

Aggarwal et al. [4] investigated water use data from Water Services Department for June 1990, 1995, and 2000. The monthly average water consumption was 17990, 16328, and 18253 gallons per single household, respectively. Household sizes during this period ranged from 2.7 to 3.0 persons/household, such that the average daily consumption per person is estimated to be roughly 180 gallons/person/day in June. Their results also show that each 1°F rise in nighttime temperature increases monthly water consumption by 2.2%/°C (1.4%/°F) for an average single-family residence.

Finally, Breyer et al. [5] investigated the water consumption in Phoenix during the summer months from June to August between 2000 and 2008. The study estimated the average water use per household is 61.89 kL (16350 gallons) for the three summer months (an average of 0.57 kL or 178 gallons per day). The results show a household water consumption sensitivity to air temperature of 3.3%/°C (1.8%/°F).

Using the estimated 178 gallons per day per Phoenix household during the summer months and approximately 600k households in the City of Phoenix, more than 3B gallons of water are used in residential households over the City of Phoenix each summer month. With an air temperature sensitivity of residential water use of about 1.8%/°F, if we can achieve a uniform cooling of 0.5°F throughout the summer across the City of Phoenix, we might expect to avoid on the order of 28M gallons of residential water use per summer month, which could amount to more than 100M gallons over the entire summer. There would likely be significant additional savings related to commercial and industrial properties.

### 3.2 Energy Consumption and Air Conditioning Savings

We explored two methods to estimate the potential air conditioning energy savings associated with ambient temperature reductions that may result from CP. These methods were an energy modeling approach and a sensitivity-based empirical estimate. Both required first estimating diurnal temperature impacts of CP across the entire year.

#### *Energy modeling approach*

We used the EnergyPlus energy simulation software tool to assess the impact of higher $T_{air}$ on air conditioning use. To do so, we developed 48 archetype single-family residential building models to represent the residential building stock of Phoenix. We used a factorial experiment design in which we characterized the entire building stock as falling into three vintage classes, two size ranges, two income levels (reflected in assumptions about occupant behavior and construction characteristics), two occupant types (schedules), and two nominal building orientations (N-S vs. E-W). We used census data to estimate percentages of households in

each census tract that fell into each of these archetypes and scaled the model results accordingly. Models were then validated against actual energy consumption data at the census tract level. We used a weighted average of the archetype energy consumption to determine typical residential energy use patterns for the City of Phoenix.

In addition to building design and occupancy details, building energy simulations require a weather data file to drive the simulations. In most cases, a “typical meteorological year” (TMY) is used to specify typical hourly weather conditions (temperature, humidity, solar radiation, and wind speeds) over every hour of the year [6].To explore the energy use sensitivity of our residential archetype buildings to perturbations in $T_{air}$ that might result from widespread deployment of CP, we developed a perturbed weather profile that used TMY data for Phoenix, with diurnal air temperature reductions based on measurements discussed in section 1.

Due to security and staffing limitations, microclimate measurements could not be performed throughout the night or the year. Daytime $T_{air}$ measurements were recorded on October 21 (Table 6). $T_{air}$ differences for the overnight hours, however, were estimated to be the same as the measured differences in surface temperatures. This $T_{air}$ perturbation profile (difference between $T_{air}$ over CP and conventional asphalt areas) for October 21$^{st}$ is shown in Figure 12.

Estimates of the impact of CP on air conditioning energy use, of course, require estimates of temperature conditions throughout the year. Since the mechanism of $T_{air}$ reduction is linked to $T_{surf}$ reductions through changes in absorbed solar radiation, it is reasonable to hypothesize that $T_{air}$ impacts of CP will roughly scale with the intensity of incoming solar radiation, being largest in summer and smallest in winter. So, to estimate $T_{air}$ reductions across the year, we scaled the perturbation profile for October by the ratio of solar radiation intensity. For example, suppose the solar radiation at 1 pm local time in June is approximately 25% higher than at 1 pm local time in October. In that case, the estimated temperature perturbation in June will be 25% higher than the estimated temperature perturbation in October. It is a highly simplified estimate of $T_{air}$ profiles throughout the year but provides a practical means of extrapolating limited measurements. Averaged over all hours of the summer, the resulting $T_{air}$ perturbations associated with CP are 0.55 °F. As expected, maximum projected diurnal $T_{air}$ reductions are found in July with a diurnal average of 0.59 °F.

The $T_{air}$ perturbation profile is then applied to Phoenix's regular TMY (climate normal) file prior to simulating the residential energy consumption impacts of widespread CP throughout residential neighborhoods.

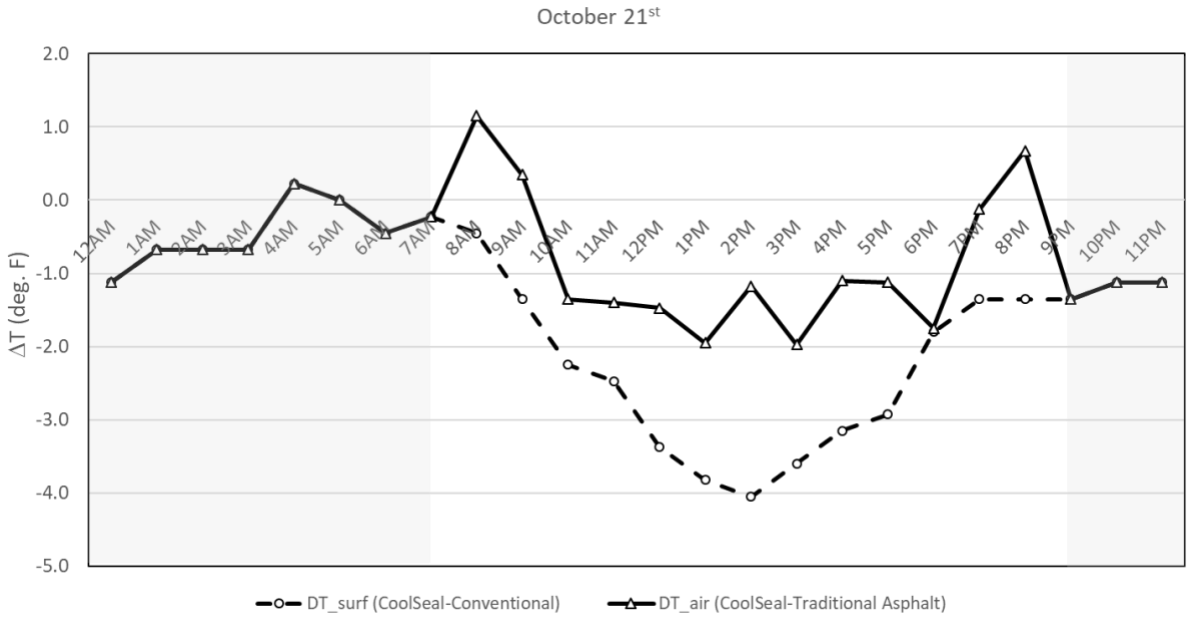


**Figure 12**. An example of a daily profile of the air temperature and surface temperature perturbations (in *°F*) for cool pavement vs. control paving neighborhoods for October 21st. The air temperature difference during the night hours (8 pm to 8 am) follows the trend of the difference in the surface temperature.

The annual hourly temperature perturbation profile was added to the TMY weather data file to create a modified weather file for running building energy simulations. All archetype buildings were simulated with the original TMY file and the updated TMY file based on the projected temperature reductions associated with CP. The annual electricity consumption estimates for the 48 archetypes were mapped to the approximate 600k households in the City of Phoenix. We estimate that Phoenix households spend more than $300M on air conditioning over a typical summer. In the scenario where CP is applied across the entire City of Phoenix, the resulting $T_{air}$ reductions are estimated to save about $10M in avoided residential air conditioning costs annually.

### *Statistical sensitivity analysis*

Prior studies have found that the residential (total) electricity use sensitivity to $T_{air}$ is around 3% per °F [7][8][9]. A typical home electric bill in Phoenix ranges from $300 to $400 per month during the summer [10][11]. Based on the estimates of average summer $T_{air}$ reductions of more than 0.55 °F associated with widespread deployment across the Phoenix area, one might expect up to a 1.6% reduction on a representative electric bill of $350/month for the five air-conditioning intensive months of May-Sep, the anticipated energy savings of this 0.55 °F $T_{air}$ reduction would be roughly $34 per household for the summer. With more than 600k households in the City of Phoenix, the potential residential energy savings associated with CP would be more than $20M. Considering both methods, we expect the annual avoided air conditioning costs across the City of Phoenix to be $10M-20M. This estimate is consistent with The Nature Conservancy's (TNC) results. In a study on the costs of inaction related to climate change [12], TNC used SRP estimates that a single °F increase in $T_{air}$ in the summer months (May-Oct) could increase average summer residential bills by $64. Scaling this by the estimated 0.55 °F cooling associated with CP, the potential avoided residential air conditioning energy use would be about $21M.

We conclude that widespread deployment of CP could save City of Phoenix households $10M-$20M annually. These estimates inherently include a high level of uncertainty as year-round hourly $T_{air}$ effects of CP have yet to be measured. Nevertheless, the results offer a window into the magnitude of potential air conditioning energy savings associated with the widespread deployment of CP. It is worth noting that these estimates do not include savings in the commercial building sector and are based on comparing CP to conventional aged pavement. A better comparison would be to explore the $T_{air}$ differences between neighborhoods sealed with a conventional black seal vs. the CP.

## 4. Impact of Cool Pavement on Human Health

Numerous questions arise as to what the impacts of CP could be on human health depending on the time of day. These questions often relate to direct impacts on the human body due to changes in different temperatures or reflected ultraviolet (UV) radiation from the pavement. Here, we present brief methods and results related to both questions.

First, the optimal assessments for answering questions around the impact of changing the surface properties on the human body involve applications of human energy balance modeling (summing the overall heat gains and losses to/from the human body) over time in different environments. We applied the human energy balance modeling approach (Cramer and Jay, 2019) to determine the needed heat loss to achieve thermal balance at the four observed times, comparing the CP to the control site and areas over the CP with tree shade (4 stops). A lower required heat loss indicates a safer environment, indicating the body is closer to thermal balance.

Results show that a person's heat loss needs were similar between the asphalt and CP (sun-exposed and shaded) in the morning and evening (Figure 13). In the daytime, heat loss requirements were, on average, 12 and 13 $Wm^{-2}$ higher over CP at 12 pm and 4 pm, respectively, indicating higher heat stress when standing on the reflective coating. At 4 am, there was no difference; at 8 pm, the heat loss requirements were 4 $Wm^{-2}$ higher over the asphalt, indicating a slightly higher heat risk. However, these values are within the sensor accuracy readings.

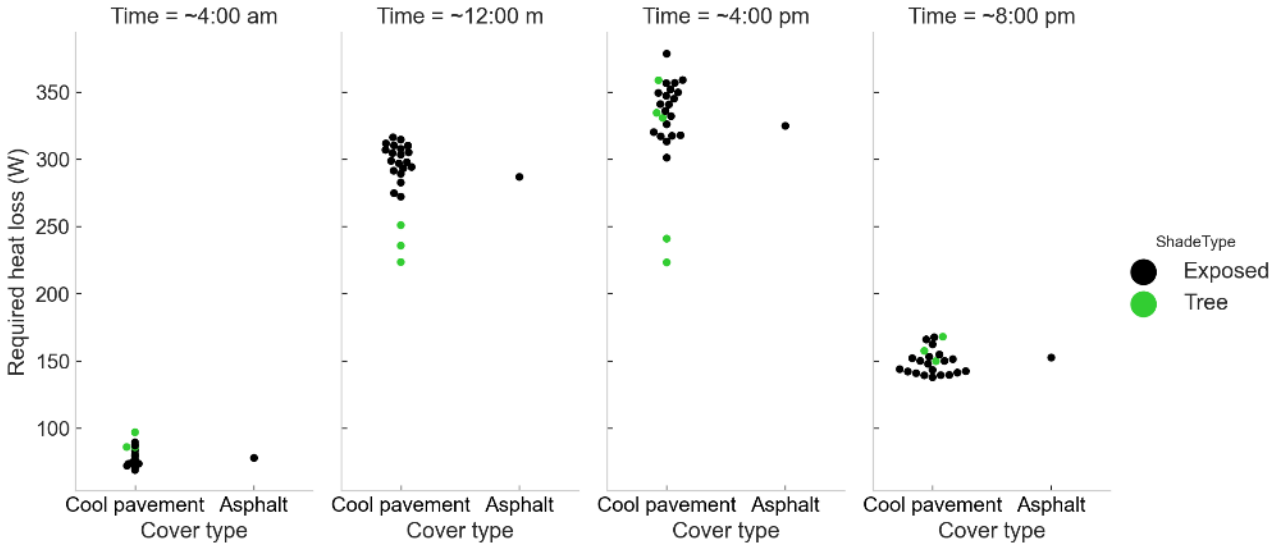


**Figure 13**: Required heat loss in W over Cool Pavement and conventional aged asphalt four times a day.

**Figure 14**: UVI and UVB sensors pointed up and down to determine the surface reflectivity over the CoolSeal. The same process was repeated over asphalt and concrete on June 13th, 2022, between 12:30 pm and 1:30 pm local time.

Second, UVB and UV index (UVI) reflectivity measurements were taken on June 13, 2022, between 12:30 pm and 1:30 pm. UVB radiation (280–315 nm) was measured using an SKU 430 pyranometer (Skye Instruments, Llandrindod Wells, UK). The UVI was monitored with an SKU 440, an erythemally-weighted average of UVA and UVB (320–280 nm), per CIE standards. Both pyranometers are cosine corrected, with minimal errors at zenith angles up to 70°, and individually calibrated for an exposure output in W $m^{-2}$. The ratio of incoming-to-outgoing radiation was determined over three surface types: concrete, asphalt, and CoolSeal, at 1.1 m height. The sensors were mounted parallel to the ground and faced up for 5 minutes and down for 5 minutes; the ratio of the outgoing (sensor facing down) to incoming (sensor facing up) was calculated and averaged per 5-minute intervals (Figure 14).

Results provided in Table 7 show that the overall UV reflection was 5.9% on the CP, slightly lower than the reflection from the asphalt (8.8%) and concrete (6.0%), respectively. The UVB reflection values for CP, asphalt, and concrete were of similar magnitude (6.7%, 8.4%, and 5.8%, respectively). These results indicate that, based on UV reflection, the CoolSeal is slightly better (reflects less, absorbs more) than the aged asphalt and similar to concrete.

**Table 7**: Reflectivity of UVB radiation (280–315 nm) erythemally-weighted UV (UVA and UVB (320–280nm)) over CoolSeal, conventional asphalt, and concrete on June 13th, 2022, taken midday (12:30-1:30 pm).

| Surface | UVI Reflectivity (%) | UVB Reflectivity (%) |
|---|---|---|
| **CoolSeal** | 5.92 | 5.65 |
| **Asphalt** | 8.80 | 8.36 |
| **Concrete** | 6.00 | 5.81 |

# 5 Non-Residential Test Beds

## 5.1 MaRTy measurements

The City of Phoenix Street Transportation Department has three roadway surfaces applied near each other as a "test bed" at their Union Hills Service Center facility in northern Phoenix. Roughly 7,000ft$^2$ of Control is located next to ~4,000ft$^2$ of CP-A and ~4,500ft$^2$ of CP-B (Figure 15a, b). To measure the effectiveness of each material under very comparable meteorological conditions (due to their proximity in comparison to neighborhoods that can be miles apart), MaRTy and spectrometer measurements were taken on September 17, 2022 (Table 8, Figure 16a, b, c). Reflectivity measurements using an ASD FieldSpec 4 Wide-Res Field Spectroradiometer were taken at roughly high sun (between 1 pm and 2 pm). MaRTy measurements were conducted every 30 minutes from 11:30 am to 7:30 pm.

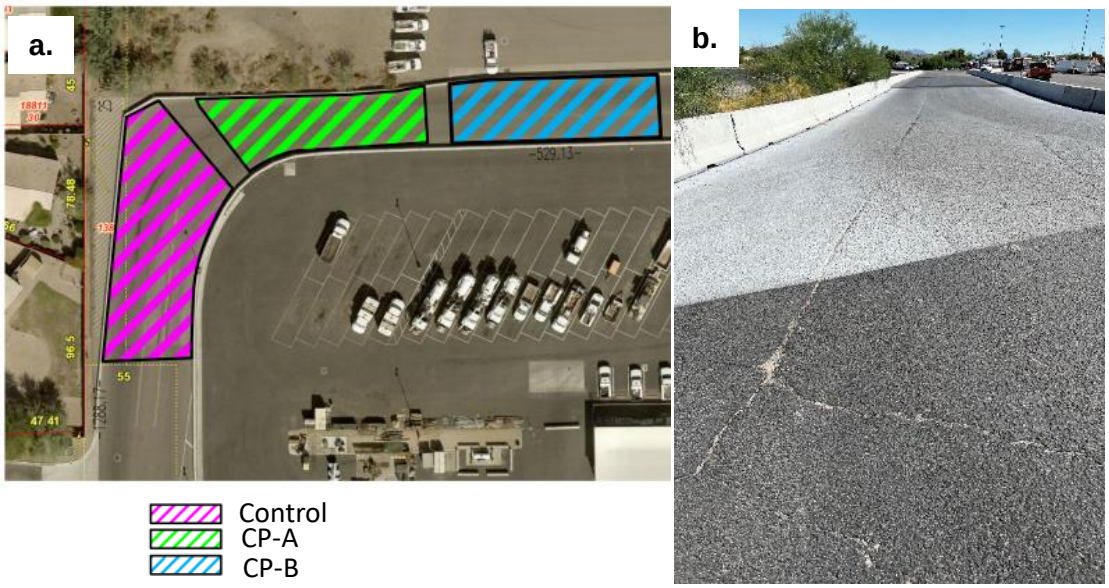


**Figure 14a.** Schematic of test bed surface locations and coverage at the City of Phoenix Transportation Department Union Hills Service Center in Northern Phoenix; and **b.** the visual differences of each surface during data collection on September 17, 2022.

**Table 8.** Conditions during measurements at the City of Phoenix Street Transportation Department Test Bed. MaRTy measurements were taken every 30mins from 11:30 am-7:30 pm. The minimum, mean, and maximum daily air temperature ($T_{air}$) is from the National Weather Service weather station at Phoenix Sky Harbor.

| | Date | Min. Daily $T_{air}$ | Mean Daily $T_{air}$ | Max. Daily $T_{air}$ |
|---|---|---|---|---|
| Test Bed | September 17th, 2022 | 77.0º F | 88.5º F | 100.0º F |


**Figure 15.** MaRTy at the Union Hills Service Center in Northern Phoenix during measurements on September 17, 2022, on **a.** the Control surface; **b.** the CP-A surface; and **c.** the CP-B surface.

Here, the control is a commonly used asphalt sealant. The average $T_{MRT}$ and standard deviations were calculated for each hour (Table App 3), followed by the difference in hourly mean $T_{MRT}$ between the Control and each respective reflective coating (Table 9). Similar patterns of $T_{MRT}$ intensification are seen across all three surfaces. Similar to results from the neighborhood transects, the reflective pavements exhibit higher $T_{MRT}$ values during the afternoon and higher insolation. $T_{MRT}$ above other reflective materials peaks at more than 5°F higher (excluding values around sunset) than that of the Control seal. The difference in performance between CP-A and CP-B relative to the Control product is of particular interest. CP-A $T_{MRT}$ is consistently lower than CP-B, albeit marginal. The significant difference around 6 pm, although included in this data output, is not a primary function of the influence of the material but rather a display of differences in incoming solar radiation as the sun angle before sunset can dramatically shift shade cover and is difficult to control for. This phenomenon is apparent in the inflated standard deviations at this hour.

**Table 9.** The difference in average mean radiant temperature ($\Delta T_{MRT}$, °F) between asphalt coated in Control and CP-A/CP-B coated asphalt on September 17, 2022, at the City of Phoenix Transportation Department Union Hills Service Center in Northern Phoenix. Measurements were taken every thirty minutes starting at 11:30 am and averaged on the hour to provide hourly MRT values between 12 pm and 7 pm.

| | 12 pm | 1 pm | 2 pm | 3 pm | 4 pm | 5 pm | 6 pm | 7 pm |
|---|---|---|---|---|---|---|---|---|
| **$T_{MRT}^{CP-A} - T_{MRT}^{Control}$** | | | | | | | | |
| | +0.5 | +1.6 | -- | +2.1 | +4.6 | +5.3 | +10.8 | -0.7 |
| **$T_{MRT}^{CP-B} - T_{MRT}^{Control}$** | | | | | | | | |
| | +1.1 | +1.6 | +3.5 | +2.6 | +4.5 | +5.7 | +19.8 | -0.8 |

### 5.2 Subsurface Temperature Measurements

iButton temperature sensors were installed in the asphalt concrete layer of the three coatings and the uncoated section. A total of 16 wired sensors were placed (4 at each location). These sensors were installed at a depth of ½ inch and 3 inches from the surface to monitor changes for the project's duration. Sensors recorded the temperatures every 30 minutes, and measurements were downloaded approximately every 1.5 months. Figure 17 shows the average maximum and minimum monthly temperatures for the sensors installed ½ inch from the surface.

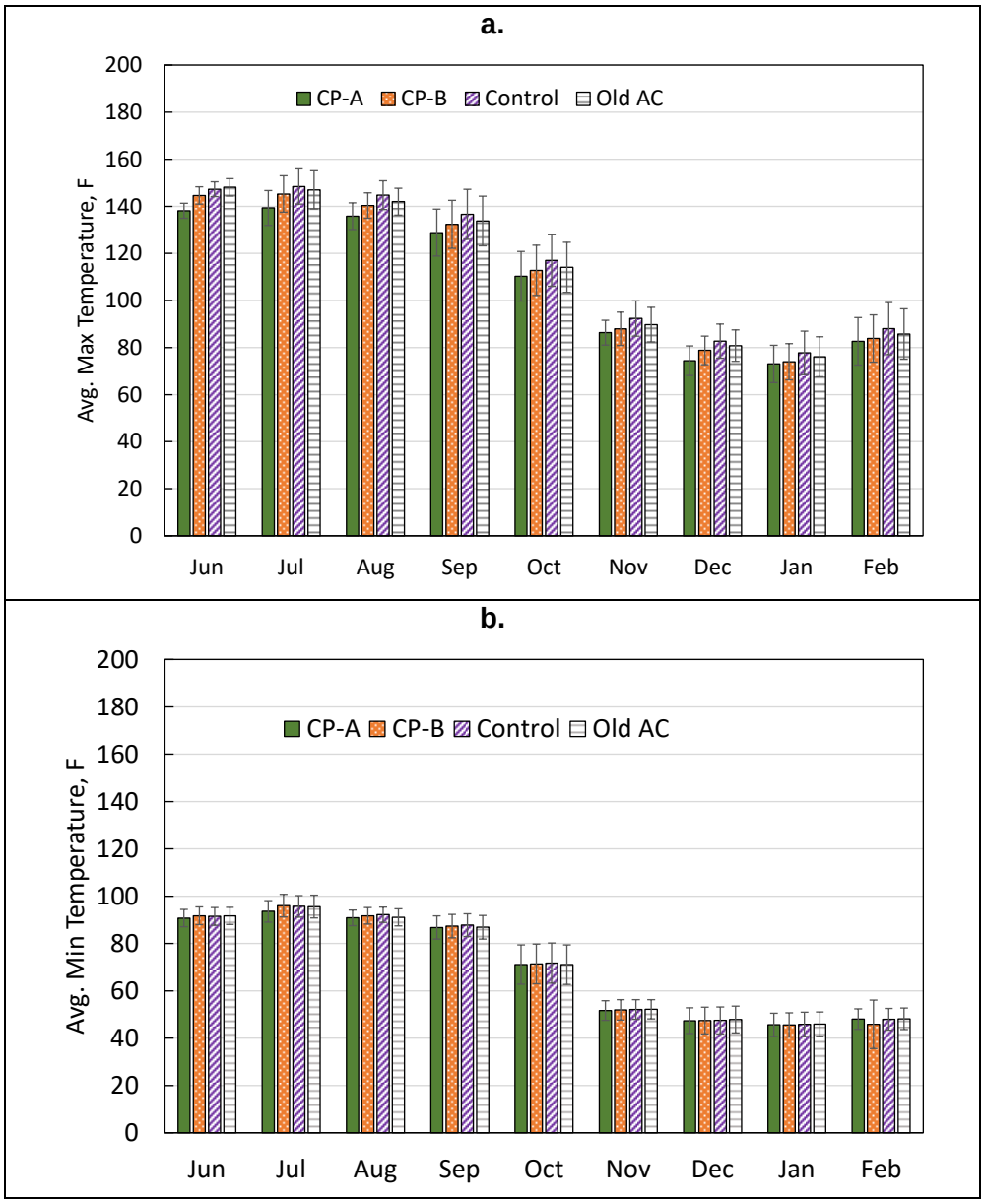


**Figure 16a.** Monthly high-temperature average; **b.** Monthly low-temperature average.

When comparing the sections with CP-A and CP-B to the Control and old pavement sections, there is a 9.6°F difference between CP-A and Control in June, but then it decreases during the winter months to a 4.0°F. Compared to the CP-B section, the difference is close to constant, with a temperature difference of approximately 3.0°F (Figure 18). Reduction of the pavement temperature can translate to a reduction in thermal stresses within the pavements, leading to a better-performing and potentially longer-lasting pavement structure.

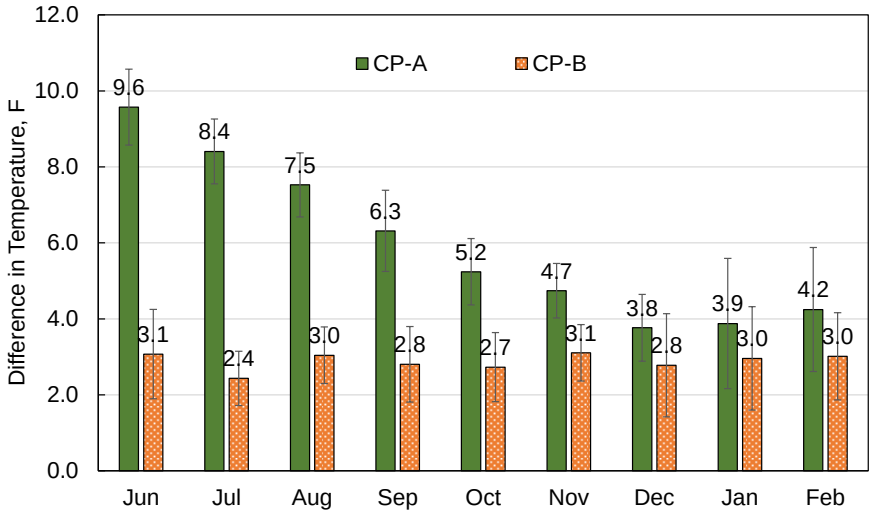


**Figure 17.** Temperature difference between Control to CP-A and CP-B.

### 5.3 Pavement Temperature Modeling

A temperature cycle from July 22, the date with the highest daily maximum temperature, was chosen to model the temperature difference between coatings (Figure 19). Pavement temperature was estimated using a model developed by Gui et al. [13]. The model considers the thermal properties of the material. The thermal properties used in the model are shown in Table 10.

**Table 10.** Material properties used in pavement temperature modeling.

| Design Data | Thermal Conductivity (W/mK) | Specific Heat Capacity (J/kgK) | Density (kg/m3) | Albedo |
|---|---|---|---|---|
| Control | 0.20 | 1,585 | 1,728 | 0.16 |
| CP-A | 0.18 | 1,272 | 1,426 | 0.28 |
| CP-B | 0.22 | 935 | 1,769 | 0.23 |

The temperature magnitude differs from the field data, but the temperature difference between Control, CP-A, and CP-B are close. For this date, the observed temperature difference between Control and CP-A was 9.0°F, and the predicted difference was 8.6°F. Compared to CP-B, the observed difference was 3.5°F, and the predicted difference was 4.0°F. It is important to note that the difference between the field measurements and the modeled temperatures might be due to the use of temperature data from a weather station in the valley that was not installed at the City of Phoenix Service Center.

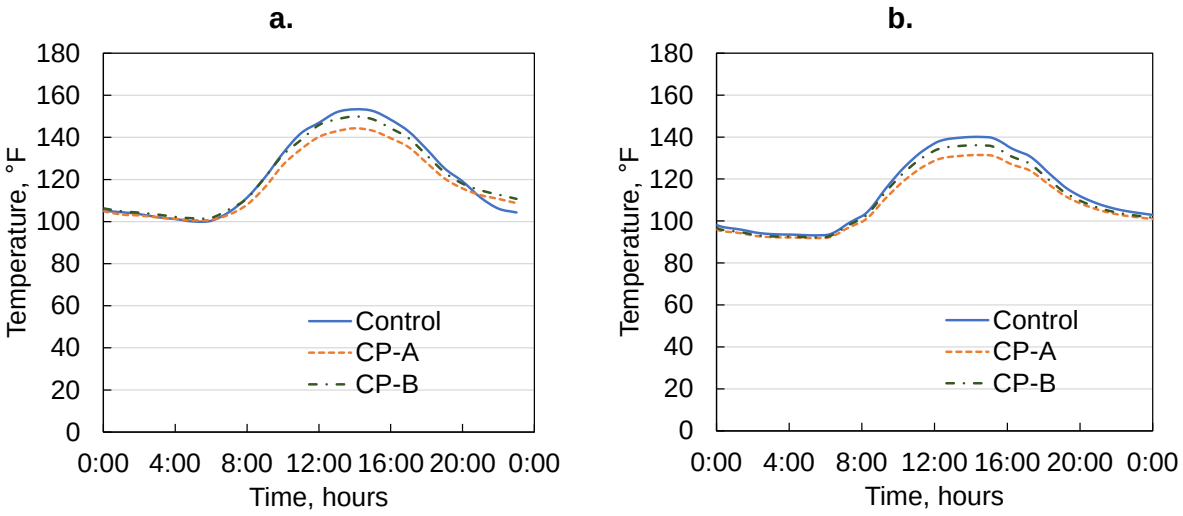


**Figure 19 a.** Field pavement temperature measurements; **b.** Modeled pavement temperature.

### 5.4 Field Visual Condition

This section visually compares the surface wear between June 2022 and March 2023. Figure 20 shows a picture of the test bed that includes the CP-A at the top of the picture and the CP-B section at the bottom. After nine months of heavy truck traffic, there is still a visible difference in color between the two sections.


**Figure 20 a.** Test section in June 2022; **b.** Test section in March 2023.

Figures 21 to 23 show pictures taken on the wheel path and the shoulders for the three test sections. As expected, there is more wear on the wheel path than the shoulders due to traffic.


**Figure 21**. Control Section – March 2023; a. Wheel path; b. Shoulder.


**Figure 22**. CP-A Section – March 2023; a. Wheel path; b. Shoulder.


**Figure 23**. CP-B Section – March 2023; a. Wheel path; b. Shoulder.

Figure 24 shows a picture of the transition between the Control and CP-A right at the curve. Since this is where the heavy trucks turn, the wear is more noticeable in both sections, as shown inside the red boundary.

Figure 25 shows the difference in color shade from the original installation in June 2022 to pictures taken in January 2023. This analysis shows that Control has become 21% lighter while the CP-A and CP-B got darker by 17% and 13%, respectively.

**Figure 24**. CP-A/Control Section, March 2023.

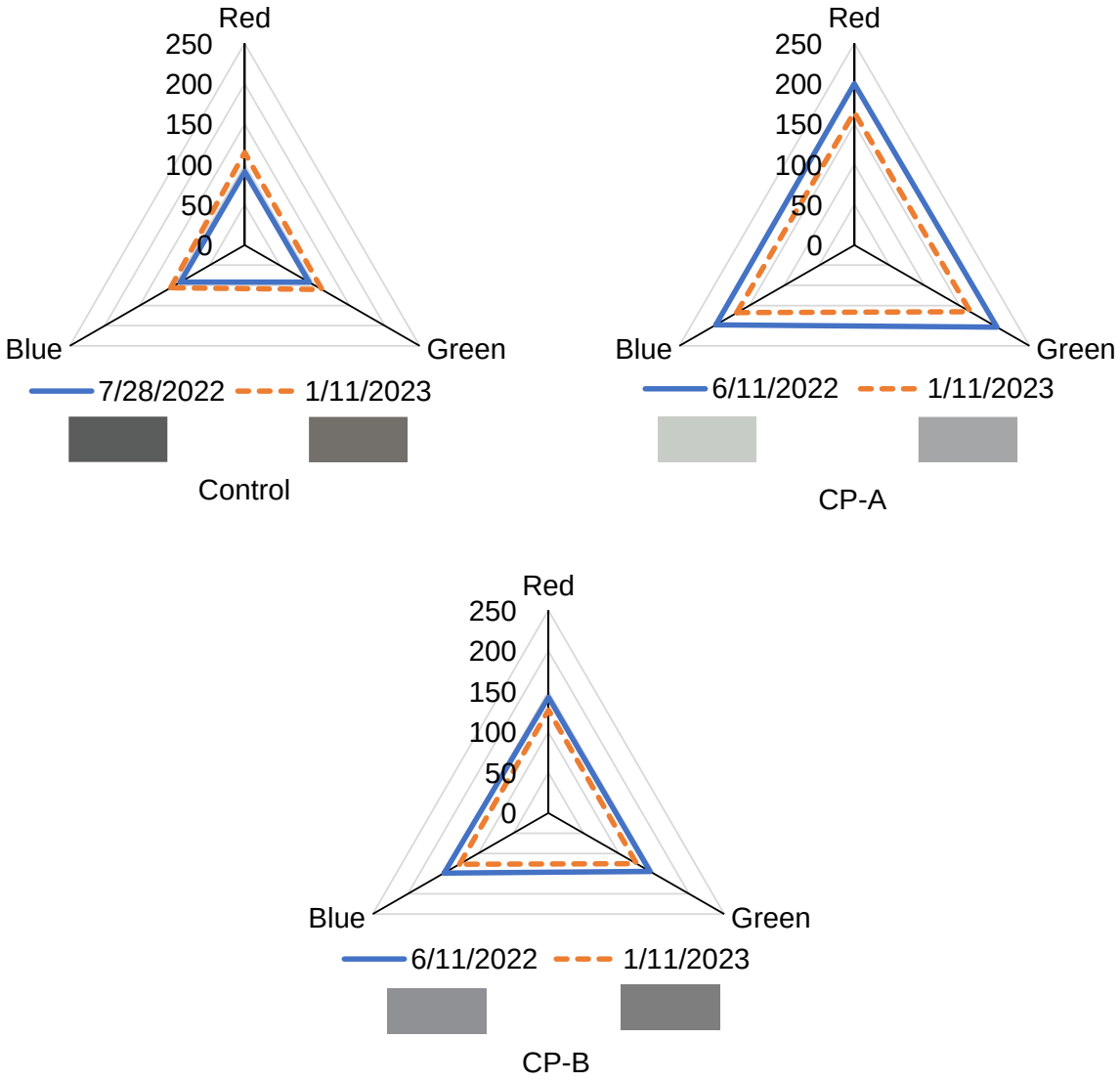


**Figure 25.** Changes in color from the original condition in 2022 to pictures taken in January 2023.

## 6 Lab testing

### 6.1 Future impact on Reclaimed Asphalt Pavement (RAP) mixes: Objective

The main objective of this part of the study was to identify if there is a detrimental effect of using the millings from pavement surfaces coated with CP coatings as reclaimed asphalt pavement (RAP). Two hot mix asphalt concrete samples were fabricated to evaluate the potential effect of using RAP sources from pavement millings with cool pavement coatings. Two performance tests were conducted: a dynamic modulus and an indirect tension test (IDT).

### 6.1.1 Mix Design

The asphalt concrete mix used in the laboratory testing experiment was a MAG/EVAC-½ in Marshall mix design with the properties shown in Table 11 and aggregate gradation shown in Figure 26.

**Table 11.** Summary of Mix Design Properties.

| Design Data | |
|---|---|
| Pb | 5.30 |
| Pbe | 4.78 |
| % Air Voids | 4.0 |
| % VMA | 15.0 |
| % VFA | 73.5 |
| Dust/Binder | 1.1 |

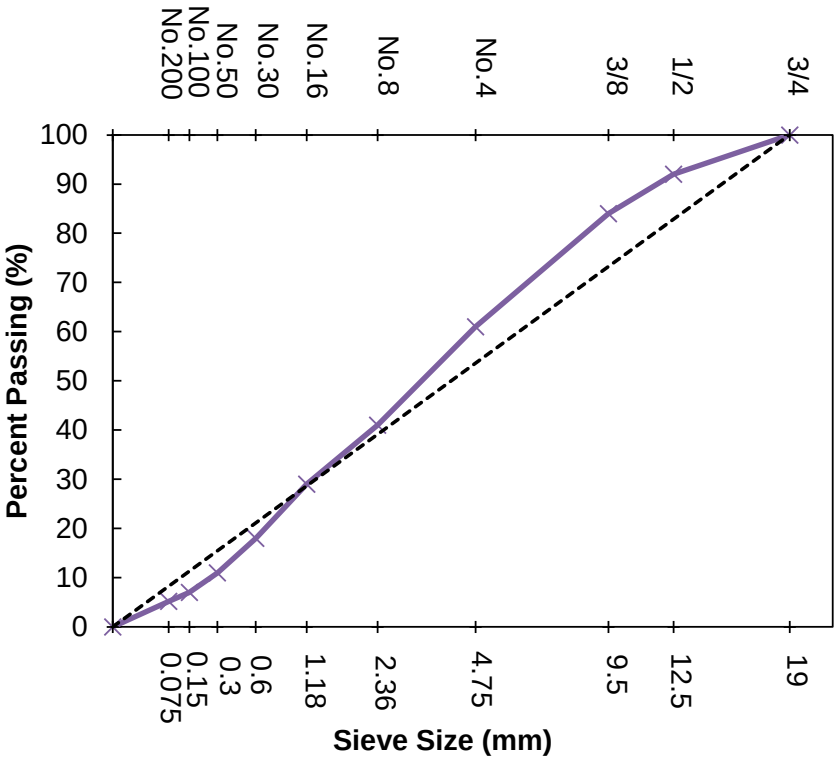


**Figure 26.** Mixture gradation.

### 6.1.2 Sample Preparation

The samples were prepared by the field mix collected from the Southwest asphalt concrete plant. To simulate RAP, Superpave gyratory plugs were fabricated and coated with either Control, CP-A, or CP-B and then placed in the oven for ten days at 85 °C. This process is commonly used in laboratory settings to age asphalt concrete samples. Figure 27 shows an example of the CP-A-coated gyratory plug. After aging the samples in the lab (Lab RAP), 20% by weight of the lab RAP samples were heated and mixed with the "fresh" field mix to produce the new gyratory plugs for testing.

**Figure 27.** Gyratory plug preparation before placing it in the oven for aging.

### 6.1.3 Test Methods and Results

***Dynamic Modulus Test***

Temperature and frequency sweep tests were performed per the AASHTO T342 protocol. The testing measured the dynamic modulus, |E*|, at temperatures of 4.4, 21.1, and 37.8°C and 25, 10, 5, 1, 0.5, and 0.1 Hz frequencies. Test samples were compacted to a height of 178 mm (7 in) and a diameter of 150 mm (6 in) via the Superpave gyratory compactor. After the samples had cooled from compaction, they were cored and cut to a final testing geometry of 100 mm (4 in) x 150 mm (diameter x height). The bulk density of these samples was then measured and used to calculate air void contents, which were 6.5 ± 0.5%. The most common method to report dynamic modulus data is the mastercurve function, which is named so because it shows the joint effects of temperature and frequency on the modulus of asphalt concrete.

The |E*| values for the mixtures are summarized in the form of dynamic modulus mastercurve functions in Figure 28. The dynamic modulus data are shown in both log-log and semi-log scales, so any differences in the moduli at high and low temperatures can be observed. Overall, it is seen that the modulus values for Control and CP-A are very similar. CP-B exhibits slightly lower modulus values at 37.8°C and higher at 4.4°C. The average percent difference in |E*| across all temperatures and frequencies is summarized in Tables 12 and 13. The results show a range in average difference from the control case between 14% softer and 2% stiffer for the CP-A and between 10% softer and 14% stiffer for the CP-B.

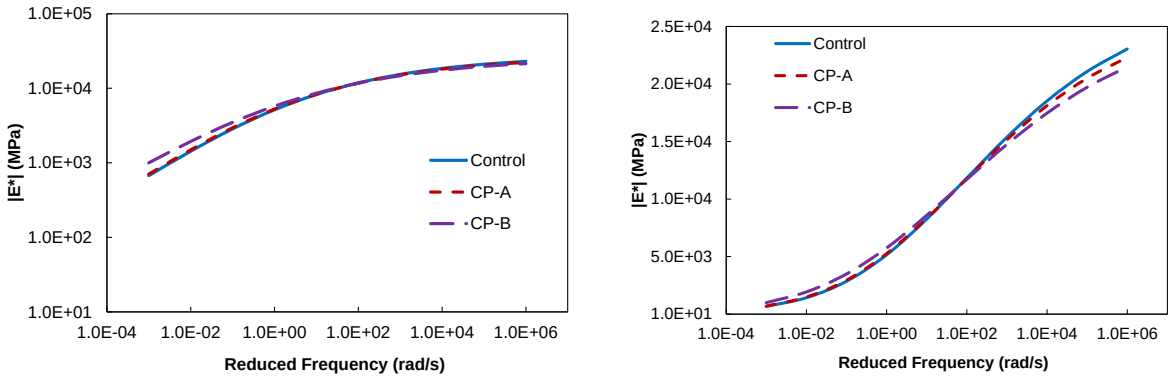


**Figure 28**. Log-log scale dynamic modulus mastercurve (left), Semi-log scale dynamic modulus mastercurve. (right).

**Table 12**. Percent Difference in Modulus between Control and CP-A.

| Frequency | Temperature | | |
|---|---|---|---|
| | 4.4 | 21.1 | 37.8 |
| 25 | -2% | -1% | -11% |
| 10 | -2% | 0% | -12% |
| 5 | -2% | 0% | -13% |
| 1 | -1% | 1% | -14% |
| 0.5 | -1% | 1% | -14% |
| 0.1 | 0% | 2% | -13% |

**Table 13** – Percent Difference in Modulus between Control and CP-B.

| Frequency | Temperature | | |
|---|---|---|---|
| | 4.4 | 21.1 | 37.8 |
| 25 | -6% | -1% | -10% |
| 10 | -5% | 1% | -9% |
| 5 | -5% | 2% | -8% |
| 1 | -3% | 6% | -4% |
| 0.5 | -2% | 8% | -2% |
| 0.1 | 1% | 14% | 6% |

An ANOVA and statistical t-test were performed at a 95% confidence level to verify the significance of the results. The ANOVA was used to compare the difference between all means and evaluate the significance of the total differences. Results show no significant difference between the means. The t-test was performed to compare individual cases to the Control mixture. The null hypothesis for the t-test was that the |E*| difference between the cases is zero. Results show that the null hypothesis cannot be rejected, and there is no evidence that the differences between Control to CP-A and Control to CP-B are significant. The tables are in the appendix (Tables App 5-8).

### *Indirect Tension Test*

The indirect tension (IDT) strength test is performed by applying a constant displacement rate along the diametrical axis of a cylindrical sample. There is currently no AASHTO standard for this method in fatigue, but generally, the parameters specified in the AASHTO T322 test protocol are followed. In this test, a specimen of 100 – 150 mm (4 – 6 in) diameter and not more than 63 mm (2.5 in) thickness is loaded at a constant rate of 50 mm/min (2.0 in/min) until it fails. The test is generally performed at or near 25°C (77°F). Four samples were tested for each mixture. The average air voids for these samples were 8.4% (Control), 8.2% (CP-A), and 8.0% (CP-B). Even though the air voids in these samples were higher than expected, they are comparable to each other and within the typical range of ± 0.5%. Figure 29 displays the tensile strength calculated for each mixture. The results

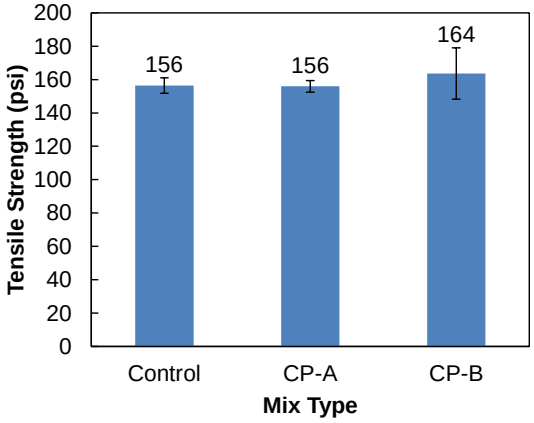


**Figure 29**. IDT tensile strength results.

show that the tensile strength is the same for Control and CP-A (156 psi). CP-B samples showed an increase in tensile strength by 5% (164 psi). Both cool pavement coatings increased the fracture energy at failure by 15%, and the total fracture energy decreased by 1% and 6% for CP-A and CP-B samples, respectively (Figure 30). However, the ANOVA test for the tensile strength and fracture energy showed no statistical significance between all three cases.

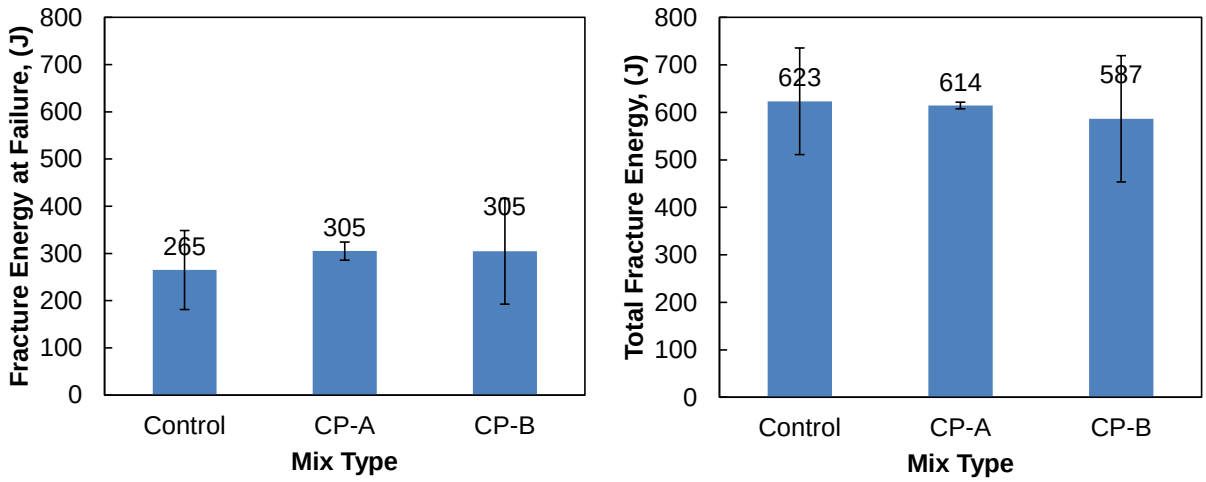


**Figure 30.** IDT fracture energy at failure and total fracture energy.

### *Hamburg Wheel Tracking Test*

The Hamburg Wheel Tracking Device, HWTD (AASHTO T324), is used to evaluate rutting and stripping potential. The HWTD tracks a loaded steel wheel back and forth directly on an HMA sample while the unrecoverable deformation is recorded. The HWTD is designed to accommodate cylinders and is desired to test two replicates simultaneously. A 47 mm (1.85 inches) wide steel wheel is commonly tracked across water-submerged samples for 20,000 cycles (or until 20 mm of deformation occurs). The water bath temperature varies according to different agencies but is generally between 50 to 60°C (122 to 140°F). Rut depth is measured continuously with a series of LVDTs on the sample.

One sample for each mixture was fabricated for this test. The air voids for the mixes were 7.7%, 7.8%, and 7.7% for the Control, CP-A, and CP-B samples, respectively. These samples were tested at 131°F. The threshold deformation used by ADOT is 0.5 inches after 20,000 cycles. Figure 31 shows that none of the mixtures exceeded the threshold. Furthermore, the CP-A sample showed an increase in rutting by 18%, while the CP-B sample had a reduction in rutting by 40%. Note that all the mixtures are way below the threshold line.

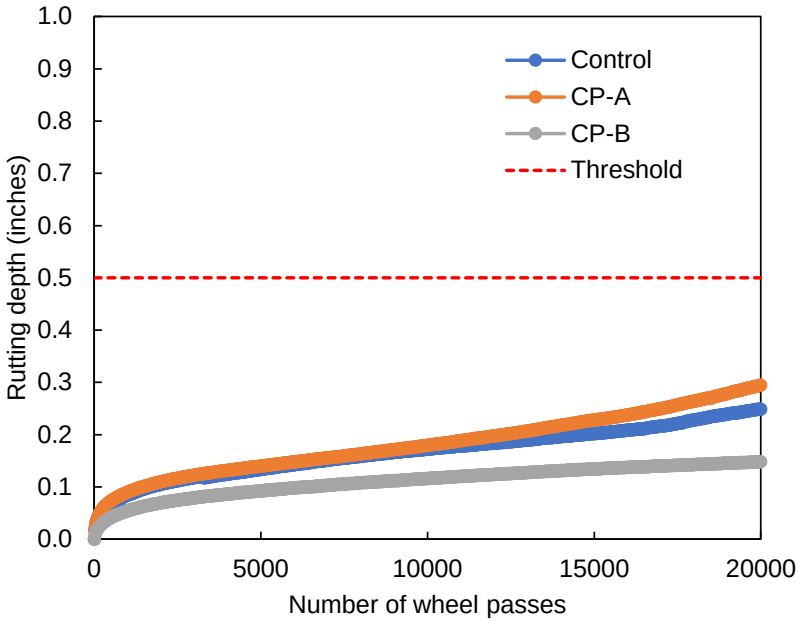


**Figure 31.** Hamburg Wheel Track test results.

### 6.1.4 Future Impact on RAP Summary

The main goal of this part of the study was to identify if there is any detrimental effect of using the millings from pavement surfaces coated with cool pavement coatings. Three performance tests were conducted: the dynamic modulus test, the indirect tension test (IDT), and the Hamburg Wheel Track test. The findings of this part of the study are as follows:

- The dynamic modulus results show a slight difference (in a positive way) between the mixtures and compared to the control, but the difference was not statistically significant. Results indicate no impact of future RAP usage on the stiffness behaviors of these mixes.
- The tensile strength results showed that the CP-B had a 5% increase in strength, which is good; the fracture energy at failure increased by 15% in both cases; the total fracture energy decreased by 1% and 6% for CP-A and CP-B samples respectively; however, the difference between the mixes was not statistically significant.
- The HWT results showed that the mixture with CP-B will provide improved resistance to rutting, but all the mixtures passed the threshold criteria.

These results indicated that adding RAP millings from pavements containing these coatings has no detrimental effects. More testing is recommended to expand the performance knowledge of these mixtures. Some of the follow-up testing may include:

- Asphalt binder extraction to study the aging behavior of the binder. It is assumed that by using these cool pavement coatings, the asphalt binder will age less and protect the underlayers.
- A complete test sweep for cracking potential can include the IDEAL CT test, C* test, Texas Overlay test, and others.

### 6.2 Surface Durability Test

A material durability test procedure was developed for laboratory-prepared mixtures. This procedure was developed and modified based on the ASTM D7000 – Standard Test Method for Sweep Test of Emulsified Asphalt Surface Treatments and the ISSA TB 100 - Laboratory Test Method for Wet Track Abrasion of Slurry Surfacing Systems. The test procedure uses a Hobart mixer with a removable 3.3 lb head brush holder. Then, a surface treatment sample is placed on a 12-inch round flat base. After that, the sample is submerged in water and tested for 405 seconds.

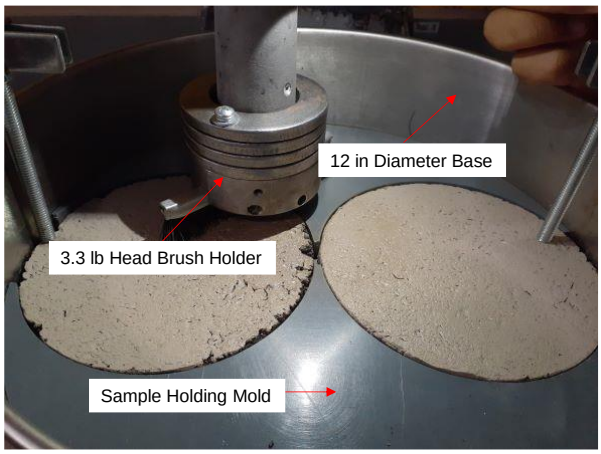


**Figure 32.** Wear test equipment setup.

For the cool pavement coatings, a mold was fabricated to hold in place two 6-inch diameter and 0.5-inch thick samples cut from gyratory plugs (Figure 32). The developed/modified test procedure is as follows:

1. ***Sample Preparation***
   a) The top and bottom of a 6-inch gyratory plug is cut to a thickness of 0.5 inch.
   b) The sample is uniformly coated with the CP coating on the uncut side.
   c) The sample is allowed to cure for at least 24 hours at ambient temperature.

2. ***Sample Conditioning***
   a) After curing, the sample is submerged in a 140°F water bath for 1 hour (Figure 33).

**Figure 33.** Samples being conditioned in the water bath at 140°F.

3. ***Testing Procedure***
   a) Take a high-resolution photo of the samples' surface before testing for image analysis.
   b) Place the two samples on the base and submerge under the heated water.
   c) To keep the water temperature as high as possible, a 250-watt heat lamp points to the base (Figure 34).
   d) The test runs for 40 min, which covers sweeping/brushing half of each of the samples; then, the samples are rotated 180° to brush the second half, and the test runs for another 40 min.
   e) The samples are dried with a towel, and photos are retaken for image analysis.

**Figure 34.** 250-watt heat lamp pointing to the samples during the test.

### *4. Image Analysis*

a) With the photos taken before and after, image analysis is done to determine the wear of the sample.
b) With image analysis, we can track the black spots (pixels) found in the photos after testing and compare them to those before testing—examples of the before and after pictures are shown in Figure 35.
c) The ratio between the black pixels of the original sample and the black pixels after the wear test will provide the percentage of wear.

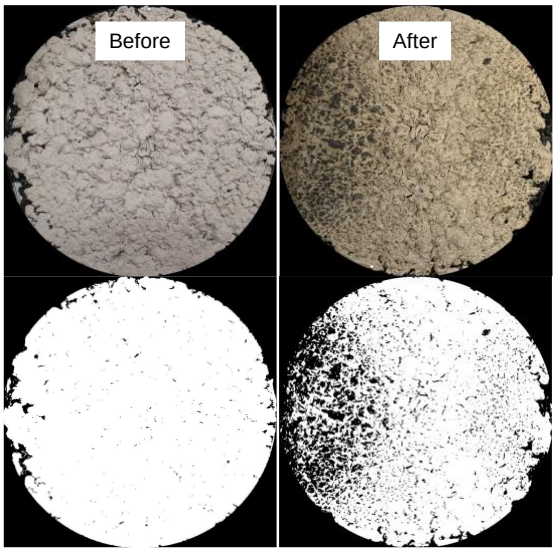


**Figure 35.** Samples before and after the wear test at the top, and the binary images for wearability analysis at the bottom.

For this test procedure, 12 samples were fabricated: six for CP-A and six for CP-B. Three cores from each coating were taken from the test bed at the City of Phoenix Service Center. The samples were tested for wearability, and Figure 35 shows images before and after the test. Table 14 summarizes the wear percentages for the lab-prepared samples and the field cores. The CP-A samples show a surface wear of 37.5% compared to a 0.9% wear for the CP-B for lab-prepared samples. The results from cores show significantly less wear than the lab-prepared samples. The Control sample had a surface wear of 2.5%, the CP-A wear was 2.4%, and the CP-B wear was 1.8%. Figure 36 shows the laboratory samples after the test. Figure 37 shows the field samples before and after the test. Note that the surface texture from the laboratory samples compared to the field samples is quite different. The difference in surface texture, the field application technique, and the longer curing time from the field might have contributed to the observed differences in surface wear between the field samples and the lab-prepared samples.

**Table 14.** Percentage Wear of Lab Samples and Field Samples.

| Frequency | Wear Percentage | |
|---|---|---|
| | Lab Samples | Field Samples |
| Control | N/A | 2.5 |
| CP-A | 37.5 | 2.4 |
| CP-B | 0.9 | 1.8 |

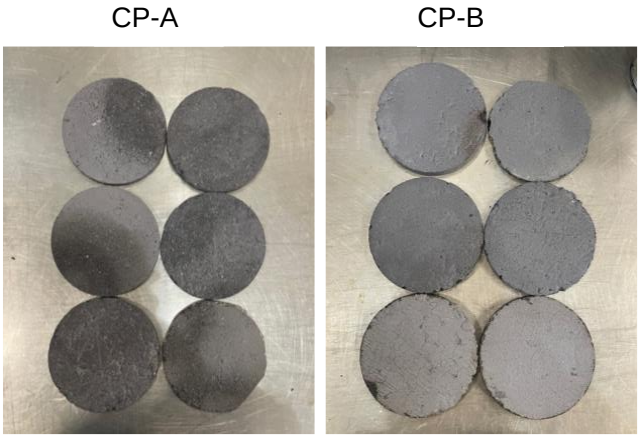


**Figure 36.** Samples after testing.

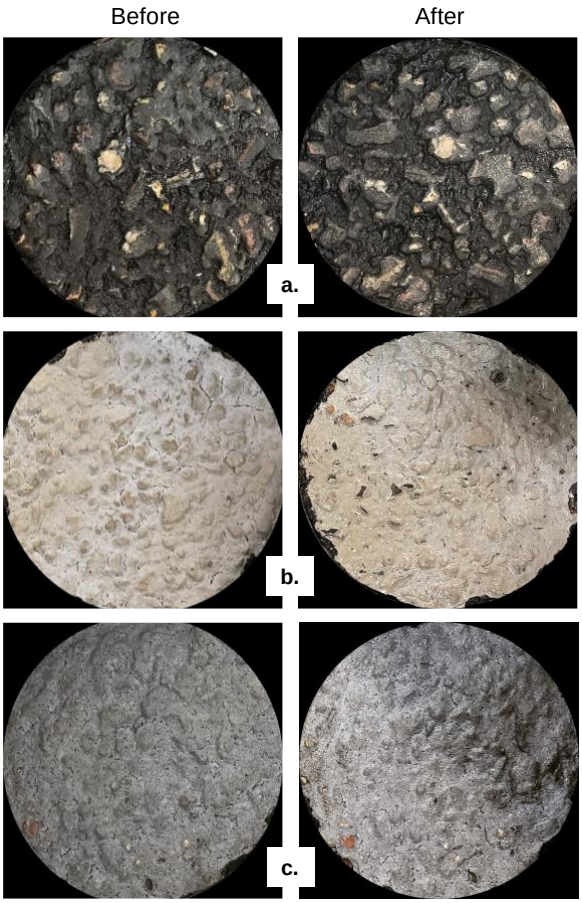


**Figure 37.** Field samples before and after the wear test. **a.** Control, **b.** CP-A; **c.** CP-B.

### 6.3 Thermal Properties Measurements and Results

#### 6.3.1 Thermal Conductivity and Specific Heat Capacity

Thermal conductivity is a physical property related to the materials' performance, which implies the energy transfer rate or heat transfer rate (Q) that occurs when bodies in contact have different temperatures. The thermal conductivity test we used is a simplified testing technique to measure the thermal conductivity of asphalt binders and has been adopted for CP coatings (Obando & Kaloush, 2022). Cylindrical samples (1.6 inch diameter by 1.2 inch height) (Figure 38) were created for Control, CP-A, and CP-B. The coatings were poured in layers and allowed to cure until the desired shape was obtained. A hole was drilled at the sample's center, reaching the specimen's mid-height. The samples were placed on a wooden frame shown in Figure 39, where type K thermocouples were inserted at the center of the samples. The setup, initially at

**Figure 38.** Thermal Conductivity and Specific Heat Samples created from CP-B, CP-A and Control respectively shown.

room temperature, was then placed in a water bath at a constant temperature of 95°F, and temperatures were recorded until the steady state temperature was reached. Thermal conductivity was then calculated and reported.

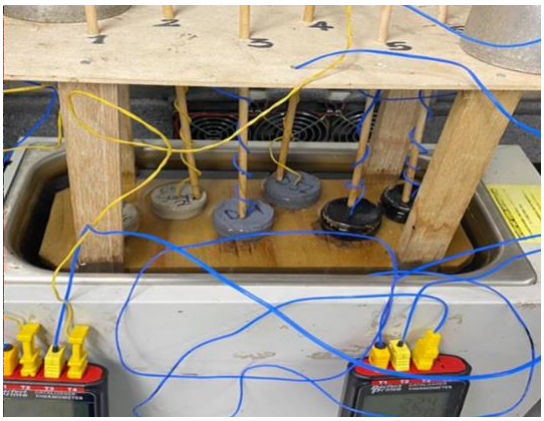

**Figure 39.** Thermal Conductivity Setup with Set up Samples. Type K Thermocouples were inserted as shown at the center and mid-height of each specimen.

As for the specific heat capacity measurements, the testing was conducted on the same samples created for thermal conductivity testing. The specific heat capacity was calculated based on the first law of thermodynamics, where the total energy rise in a system equals the increase in thermal energy plus the work done on the system. In other words, the specific heat capacity test measures the energy needed to increase a material's temperature by 1.8°F (1°C). The created samples were heated in a conventional oven for over an hour at a temperature between 140°F and 176°F. An insulating flask was used as a medium where the heated sample was submerged in room temperature water. The flask allowed for minimized energy losses between the system and the environment. Heat exchange between the water and the sample was measured, and the specific heat capacity of all the samples was calculated according to the following equation:

$$C_s = \frac{m_w * C_s * \Delta T_W + m_f * C_f * \Delta T_f}{m_s * \Delta T_s}$$

where the subscript "*w*" stands for water, "*f*" stands for flask, and "*s*" stands for specimen, *T* refers to the Temperature in °C, *C* refers to the specific heat capacity in (J.kg^(-1) K^(-1)), and *m* refers to the mass in (kg). The results of the thermal conductivity and specific heat capacity are summarized in Table 15. The samples have been tested for unaged and aged conditions, where aging has been simulated using a conventional oven at elevated temperatures (325 °F) for 5 hours.

**Table 15.** Thermal Conductivity and Specific Heat Capacity Results for all the Cool Pavement Coatings: CP-A, CP-B, and Control.

| Product | Thermal Conductivity (W/mK) | Specific Heat Capacity (J/kgK) |
|---|---|---|
| Control | 0.20 | 1,585 |
| CP-A | 0.18 | 1,272 |
| CP-B | 0.22 | 935 |
| **Aged Condition** | | |
| Control | 0.21 | 1,235 |
| CP-A | 0.22 | 841 |
| CP-B | 0.32 | 734 |

The recorded values for the thermal conductivity were similar before aging; the specific heat results show that Control conducts and stores heat more than CP-A and CP-B. As the Control has a darker color, storing more heat at the pavement's surface is relevant and is supported by

the measured temperatures in the field. Furthermore, the results show that the CP-B will be quicker to increase and decrease in temperature. As for CP-A, the coating is expected to allow less heat (lower thermal conductivity) within the pavement, resulting in lower surface temperatures when compared to the other products. Similar trends were observed for the aged samples. However, the color (reflectivity) of the products also plays a role in how the pavement will experience heat (i.e., higher reflectivity yields less surface temperature).

### 6.3.2 Expansion and Contraction Testing

For this test, CP coatings were made into beams with the same dimension as the sample used for the Bending Beam Rheometer test (ASTM D6648), as shown in Figure 40. Strain gauges were placed on the smooth sides of the beams, and thermocouples were epoxied to the surface of the beams. The samples were placed inside a conditioning chamber where thermal cycling was subjected to the specimens.

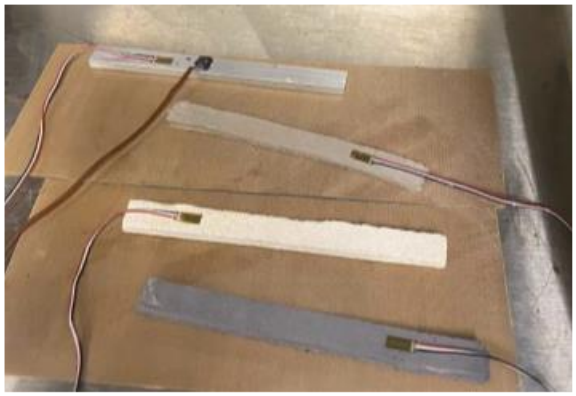

**Figure 40.** Expansion and Contraction Testing Samples.

The change in strains measured by the strain gauges at different temperatures was recorded using LabVIEW, and the coefficient of thermal expansion and contraction (CTE) was calculated according to the following equation:

$$\alpha = \frac{\Delta T}{\Delta \epsilon}$$

Where $\alpha$ is the linear coefficient of expansion in $°F^{-1}$, $\Delta T$ is the change in temperature between cycles measured at the sample's surface in $°F$, $\Delta \epsilon$ is the change in strain measured in response to the thermal cycles, in/in. The results are summarized in Table 16.

**Table 16.** Coefficient of Thermal Expansion and Contraction for all the Cool Pavement Coatings: CP-A, CP-B, and Control.

| Product | Expansion-Contraction Coefficient (/°F) |
|---|---|
| Control | 2.84E-05 |
| CP-A | 2.17E-05 |
| CP-B | 9.99E-06 |

The results of this test are essential to further understand the thermal susceptibility of the three products. A lower CTE refers to a lower temperature susceptibility of the material and a lower potential to crack. The results show that Control had the highest coefficient, while CP-B had the lowest.

### 6.4 Solar Reflectance Data Results

Small paving samples (nominally 2” square and <1” thick) were brought to the laboratory for analysis. We used the Perkin Lambda 950 UV-Vis spectrometer in the Eyring Materials Center to measure spectral reflectivity across the solar spectrum. The Lambda 950 UV/Vis/NIR is a double beam, double monochromator, all-reflecting optical system that operates in the UV, visible (vis), and near infra-red (NIR) spectral range. The spectrometer uses Deuterium and tungsten Halogen light sources. Automatic source change occurs during monochromator slewing; programmed optical filters also perform automatic filter change. The system was used in conjunction with an integrating sphere to measure the solar reflectance of each sample in wavelengths from 285 to 2500 nm at 5 nm steps (a total of 444 measurements). Note that this wavelength range includes roughly 95% of the energy content of solar radiation. Solar reflectance was then calculated by dividing the total amount of reflected solar radiation by the total amount of incident radiation, using the AM1.5G standard atmosphere (see ASTM G173-03) to describe the typical solar spectrum.

Results are displayed in Figure 41. On average, CP-B had a solar reflectance of 30.29%, CP-A 38.62%, and Control 3.57%.

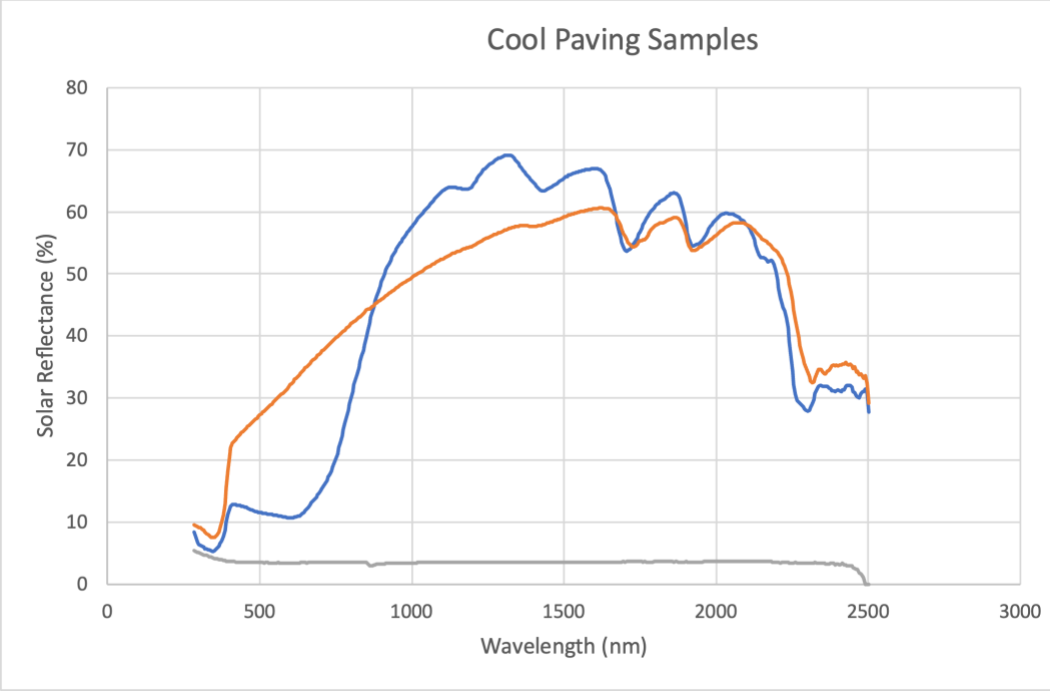


**Figure 41.** The solar reflectance of the testing samples in the lab. Blue: CP-B; Orange: CP-A; Grey: Control.

## 7 References


[1] Balling, R. C., & Gober, P. (2007). Climate variability and residential water use in the city of Phoenix, Arizona. *Journal of Applied Meteorology and Climatology*, 46(7), 1130-1137. https://doi.org/10.1175/JAM2518.1.

[2] Guhathakurta, S., & Gober, P. (2007). The impact of the Phoenix urban heat island on residential water use. *Journal of the American Planning Association*, 73(3), 317-329. https://doi.org/10.1080/01944360708977980.

[3] Guhathakurta, S., & Gober, P. (2010). Residential land use, the urban heat island, and water use in Phoenix: A path analysis. *Journal of Planning Education and Research*, 30(1), 40-51. https://doi.org/10.1177/0739456X10374187.

[4] Aggarwal, R. M., Guhathakurta, S., Grossman-Clarke, S., & Lathey, V. (2012). How do variations in Urban Heat Islands in space and time influence household water use? The case of Phoenix, Arizona. *Water Resources Research*, 48(6). https://doi.org/10.1029/2011WR010924.

[5] Breyer, B., Chang, H., & Parandvash, G. H. (2012). Land-use, temperature, and single-family residential water use patterns in Portland, Oregon and Phoenix, Arizona. *Applied Geography*, 35(1-2), 142-151. https://doi.org/10.1016/j.apgeog.2012.06.012.

[6] Thevenard, D. J., & Brunger, A. P. (2002). The development of typical weather years for international locations: Part I, algorithms. *Ashrae Transactions*, 108, 376.

[7] Bartos, M., Chester, M., Johnson, N., Gorman, B., Eisenberg, D., Linkov, I., & Bates, M. (2016). Impacts of rising air temperatures on electric transmission ampacity and peak electricity load in the United States. *Environmental Research Letters*, 11(11), 114008. https://doi.org/10.1088/1748-9326/11/11/114008

[8] Sailor, D. J., & Pavlova, A. A. (2003). Air conditioning market saturation and long-term response of residential cooling energy demand to climate change. *Energy*, 28(9), 941-951. https://doi.org/10.1016/s0360-5442(03)00033-1

[9] Ramirez-Aguilar, E.A., J. Anand, M. Alhazmi, and D.J. Sailor .(2023). A data-driven approach to validate and contextualize archetype-based building energy models with census-tract information of population demographics and neighborhood characteristics", to be presented as an oral presentation (by EAR) at the 11th International Conference on Urban Climate (ICUC-11), sponsored by the IAUC, Sydney, AUSTRALIA, 28 Aug – 1 Sep.

[10] https://americanhomewater.com/average-electric-bill-in-phoenix-during-the-summer/#:~:text=We%20can%20speak%20empirically%2C%20however,during%20the%20peak%20summer%20months

[11] www.energysage.com

[12] The Nature Conservancy, 2022. Economic Assessment of Heat in the Phoenix Metro Area, 72pp.

[13] Gui, J., Phelan, P., Kaloush, K., & Golden, J. (2007). Impact of Pavement Thermophysical Properties on Surface Temperatures. Journal of Materials in Civil Engineering. ASCE, 19(8), 683-690

## Appendix

**Table App 1.** Mean air temperature ($T_{air}$, °F) from mobile transects over asphalt and Cool Pavement (CoolSeal) at four heights (0.5m, 1.0m, 1.5m, and 2.0m) on September 6, 2022, in the Maryvale neighborhood by time. One-hour bike transects were done midday (12 pm, 1 pm), afternoon (4 pm, 5 pm), and post-sunset (8 pm, 9 pm).

| Time | Mean $T_{air}$ ± SD 0.5m | Mean $T_{air}$ ± SD 1m | Mean $T_{air}$ ± SD 1.5m | Mean $T_{air}$ ± SD 2m |
|---|---|---|---|---|
| **Traditional Asphalt** | | | | |
| 12 pm | 108.6 ± 0.6 | 107.8 ± 0.6 | 107.9 ± 0.6 | 107.0 ± 0.7 |
| 1 pm | 109.9 ± 0.7 | 109.0 ± 0.7 | 109.1 ± 0.6 | 108.2 ± 0.7 |
| 4 pm | 110.6 ± 0.9 | 109.8 ± 0.9 | 110.2 ± 0.7 | 109.3 ± 0.7 |
| 5 pm | 110.0 ± 0.4 | 109.1 ± 0.5 | 109.5 ± 0.4 | 109.0 ± 0.5 |
| 8 pm | 102.5 ± 1.0 | 102.2 ± 1.0 | 102.6 ± 0.9 | 102.1 ± 0.9 |
| 9 pm | 97.8 ± 0.6 | 97.5 ± 0.6 | 97.9 ± 0.6 | 97.4 ± 0.6 |
| **CoolSeal** | | | | |
| 12 pm | 108.2 ± 1.0 | 107.5 ± 0.9 | 107.6 ± 0.8 | 106.7 ± 0.9 |
| 1 pm | 109.6 ± 0.8 | 108.8 ± 0.8 | 108.9 ± 0.8 | 108.0 ± 0.8 |
| 4 pm | 110.8 ± 0.7 | 110.0 ± 0.6 | 110.3 ± 0.6 | 109.5 ± 0.6 |
| 5 pm | 110.0 ± 0.6 | 109.1 ± 0.7 | 109.7 ± 0.6 | 108.9 ± 0.6 |
| 8 pm | 101.9 ± 1.4 | 101.6 ± 1.4 | 102.0 ± 1.3 | 101.5 ± 1.4 |
| 9 pm | 98.1 ± 0.9 | 97.8 ± 0.9 | 98.2 ± 0.8 | 97.7 ± 0.9 |

**Table App 2.** Mean air temperature ($T_{air}$, °F) values over asphalt and Cool Pavement (CoolSeal) at four different heights (0.5 m, 1 m, 1.5 m, and 2 m) in stationary spots on October 21st, 2022, in the Maryvale neighborhood between ~7:30 am and ~8:30 pm.

| Time | Mean $T_{air}$ ± SD 0.5 m | Mean $T_{air}$ ± SD 1 m | Mean $T_{air}$ ± SD 1.5 m | Mean $T_{air}$ ± SD 2 m |
|---|---|---|---|---|
| **Traditional Asphalt** | | | | |
| 8 am | 72.1 ± 2.8 | 72.7 ± 2.2 | 72.3 ± 2.4 | 71.9 ± 2.4 |
| 9 am | 79.7 ± 1.6 | 79.5 ± 1.5 | 79.3 ± 1.5 | 78.9 ± 1.4 |
| 10 am | 84.0 ± 1.3 | 83.6 ± 1.2 | 83.3 ± 1.1 | 82.7 ± 1.0 |
| 11 am | 87.2 ± 1.0 | 86.6 ± 1.1 | 86.2 ± 1.1 | 85.7 ± 1.2 |
| 12 pm | 90.0 ± 1.0 | 89.3 ± 1.2 | 89.0 ± 1.1 | 88.2 ± 1.2 |
| 1 pm | 91.7 ± 1.0 | 91.2 ± 1.3 | 90.8 ± 1.2 | 90.2 ± 1.2 |
| 2 pm | 92.1 ± 0.7 | 91.6 ± 0.8 | 91.3 ± 0.8 | 90.5 ± 0.8 |
| 3 pm | 92.6 ± 0.8 | 92.2 ± 0.9 | 91.9 ± 0.7 | 91.2 ± 0.7 |
| 4 pm | 90.2 ± 0.6 | 90.1 ± 0.8 | 90.4 ± 0.9 | 89.9 ± 0.9 |
| 5 pm | 88.0 ± 1.0 | 87.7 ± 0.7 | 87.6 ± 0.7 | 87.3 ± 0.7 |
| 6 pm | 83.5 ± 1.6 | 83.8 ± 1.5 | 84.1 ± 1.4 | 83.9 ± 1.3 |
| 7 pm | 76.5 ± 1.3 | 77.1 ± 1.2 | 77.4 ± 1.3 | 77.3 ± 1.3 |
| 8 pm | 73.8 ± 0.6 | 74.5 ± 0.6 | 74.8 ± 0.5 | 74.4 ± 0.4 |
| **CoolSeal** | | | | |
| 8 am | 74.0 ± 2.3 | 74.0 ± 2.3 | 73.3 ± 2.2 | 72.3 ± 2.2 |
| 9 am | 80.2 ± 1.0 | 80.2 ± 1.0 | 79.7 ± 1.0 | 78.7 ± 1.0 |
| 10 am | 82.6 ± 1.1 | 82.6 ± 1.1 | 82.1 ± 1.1 | 80.9 ± 1.1 |
| 11 am | 85.7 ± 0.9 | 85.7 ± 0.9 | 85.0 ± 0.9 | 83.7 ± 1.0 |
| 12 pm | 88.4 ± 1.0 | 88.4 ± 1.0 | 87.5 ± 1.1 | 86.3 ± 1.2 |
| 1 pm | 89.8 ± 0.8 | 89.8 ± 0.8 | 88.9 ± 0.9 | 87.6 ± 1.1 |
| 2 pm | 90.9 ± 0.8 | 90.9 ± 0.8 | 90.1 ± 0.8 | 88.9 ± 1.0 |
| 3 pm | 90.7 ± 0.6 | 90.7 ± 0.6 | 89.8 ± 0.5 | 88.8 ± 0.6 |
| 4 pm | 89.6 ± 0.7 | 89.6 ± 0.7 | 88.9 ± 0.6 | 88.1 ± 0.6 |
| 5 pm | 86.9 ± 1.0 | 86.9 ± 1.0 | 86.6 ± 0.9 | 85.7 ± 0.9 |
| 6 pm | 82.4 ± 1.9 | 82.4 ± 1.9 | 82.2 ± 1.8 | 81.3 ± 1.9 |
| 7 pm | 77.3 ± 0.9 | 77.3 ± 0.9 | 77.1 ± 1.0 | 76.1 ± 1.0 |
| 8 pm | 75.6 ± 0.5 | 75.6 ± 0.5 | 75.1 ± 0.5 | 73.9 ± 0.5 |

**Table App 3.** Mean Radiant temperature ($T_{MRT}$, °F) values over Control, CP-A, and CP-B coated asphalt on September 17, 2022, at the City of Phoenix Transportation Department Union Hills Service Center in Northern Phoenix. Measurements were taken every thirty minutes starting at 11:30 am and averaged on the hour to provide hourly $T_{MRT}$ values between 12 pm and 7 pm.

| Time | Mean $T_{MRT}$ ± SD Control | Mean $T_{MRT}$ ± SD CP-A | Mean $T_{MRT}$ ± SD CP-B |
|---|---|---|---|
| 12 pm | 148.6 ± 0.6 | 149.1 ± 0.7 | 149.7 ± 0.8 |
| 1 pm | 148.0 ± 0.3 | 149.6 ± 0.6 | 149.6 ± 2.1 |
| 2 pm | 147.7 ± 1.2 | 147.7 ± 0.5 | 151.2 ± 1.9 |
| 3 pm | 151.8 ± 0.7 | 153.9 ± 0.4 | 154.4 ± 0.3 |
| 4 pm | 148.0 ± 1.9 | 152.6 ± 1.8 | 152.5 ± 1.4 |
| 5 pm | 137.9 ± 4.3 | 143.2 ± 3.5 | 143.6 ± 3.9 |
| 6 pm | 102.3 ± 15.5 | 113.1 ± 16.9 | 122.1 ± 8.8 |
| 7 pm | 82.9 ± 0.9 | 82.2 ± 1.5 | 82.1 ± 1.5 |

**Table App 4.** Dynamic modulus results for mixtures containing Control.

| Temp (°C) | Freq (Hz) | Dynamic Modulus, \|E*\| (MPa) | | | | |
|---|---|---|---|---|---|---|
| | | Repl. 1 | Repl. 2 | Repl. 3 | Aver. | Coeff. Of Var. (%) |
| 4.4 | 25 | 20838 | 21458 | 19378 | 20558 | 5.2 |
| | 10 | 19743 | 20345 | 18423 | 19504 | 5.0 |
| | 5 | 18864 | 19437 | 17642 | 18648 | 4.9 |
| | 1 | 16667 | 17127 | 15641 | 16479 | 4.6 |
| | 0.5 | 15664 | 16057 | 14708 | 15476 | 4.5 |
| | 0.1 | 13241 | 13453 | 12421 | 13038 | 4.2 |
| 21.1 | 25 | 12185 | 11974 | 11275 | 11811 | 4.0 |
| | 10 | 10776 | 10466 | 9929 | 10390 | 4.1 |
| | 5 | 9723 | 9352 | 8925 | 9333 | 4.3 |
| | 1 | 7381 | 6932 | 6713 | 7009 | 4.9 |
| | 0.5 | 6442 | 5990 | 5839 | 6090 | 5.2 |
| | 0.1 | 4488 | 4100 | 4059 | 4216 | 5.6 |
| 37.8 | 25 | 5477 | 3245 | 3000 | 3907 | 34.9 |
| | 10 | 4415 | 2512 | 2330 | 3086 | 37.4 |
| | 5 | 3695 | 2050 | 1906 | 2551 | 39.0 |
| | 1 | 2316 | 1247 | 1164 | 1576 | 40.8 |
| | 0.5 | 1848 | 998 | 934 | 1260 | 40.5 |
| | 0.1 | 1031 | 591 | 555 | 725 | 36.5 |

**Table App 5.** Dynamic modulus results for mixtures containing CP-A.

| Temp (°C) | Freq (Hz) | Dynamic Modulus, \|E*\| (MPa) | | | | |
|---|---|---|---|---|---|---|
| | | Repl. 1 | Repl. 2 | Repl. 3 | Aver. | Coeff. Of Var. (%) |
| 4.4 | 25 | 18275 | 23817 | 18222 | 20104 | 16.0 |
| | 10 | 17227 | 22677 | 17440 | 19115 | 16.1 |
| | 5 | 16398 | 21746 | 16787 | 18310 | 16.3 |
| | 1 | 14374 | 19368 | 15059 | 16267 | 16.6 |
| | 0.5 | 13468 | 18261 | 14229 | 15319 | 16.8 |
| | 0.1 | 11327 | 15544 | 12131 | 13001 | 17.2 |
| 21.1 | 25 | 10427 | 13670 | 11080 | 11726 | 14.6 |
| | 10 | 9221 | 12064 | 9784 | 10357 | 14.5 |
| | 5 | 8331 | 10867 | 8802 | 9333 | 14.5 |
| | 1 | 6379 | 8231 | 6594 | 7068 | 14.3 |
| | 0.5 | 5604 | 7187 | 5710 | 6167 | 14.4 |
| | 0.1 | 4000 | 5051 | 3895 | 4315 | 14.8 |
| 37.8 | 25 | 3256 | 3858 | 3296 | 3470 | 9.7 |
| | 10 | 2577 | 3025 | 2537 | 2713 | 10.0 |
| | 5 | 2133 | 2492 | 2055 | 2227 | 10.5 |
| | 1 | 1317 | 1547 | 1216 | 1360 | 12.5 |
| | 0.5 | 1051 | 1249 | 959 | 1086 | 13.7 |
| | 0.1 | 598 | 751 | 544 | 631 | 17.0 |

**Table App 6.** Dynamic modulus results for mixtures containing CP-B.

| Temp (°C) | Freq (Hz) | Dynamic Modulus, \|E*\| (MPa) | | | | |
|---|---|---|---|---|---|---|
| | | Repl. 1 | Repl. 2 | Repl. 3 | Aver. | Coeff. Of Var. (%) |
| 4.4 | 25 | 18774 | 19557 | 19565 | 19299 | 2.4 |
| | 10 | 17887 | 18734 | 18740 | 18454 | 2.7 |
| | 5 | 17166 | 18058 | 18065 | 17763 | 2.9 |
| | 1 | 15336 | 16320 | 16327 | 15994 | 3.6 |
| | 0.5 | 14488 | 15502 | 15511 | 15167 | 3.9 |
| | 0.1 | 12413 | 13469 | 13484 | 13122 | 4.7 |
| 21.1 | 25 | 11257 | 11930 | 11873 | 11686 | 3.2 |
| | 10 | 10030 | 10683 | 10631 | 10448 | 3.5 |
| | 5 | 9110 | 9741 | 9694 | 9515 | 3.7 |
| | 1 | 7061 | 7615 | 7581 | 7419 | 4.2 |
| | 0.5 | 6238 | 6750 | 6722 | 6570 | 4.4 |
| | 0.1 | 4520 | 4926 | 4911 | 4785 | 4.8 |
| 37.8 | 25 | 3549 | 3711 | 3325 | 3528 | 5.5 |
| | 10 | 2842 | 2969 | 2644 | 2818 | 5.8 |
| | 5 | 2380 | 2483 | 2203 | 2356 | 6.0 |
| | 1 | 1536 | 1595 | 1405 | 1512 | 6.4 |
| | 0.5 | 1260 | 1305 | 1147 | 1237 | 6.6 |
| | 0.1 | 784 | 806 | 708 | 766 | 6.7 |

**Table App 7.** Summary of ANOVA.

| Frequency (Hz) | Temperatures (°C) | | |
|---|---|---|---|
| | 4.4 | 21.1 | 37.8 |
| 25 | NS | NS | NS |
| 10 | NS | NS | NS |
| 5 | NS | NS | NS |
| 1 | NS | NS | NS |
| 0.5 | NS | NS | NS |
| 0.1 | NS | NS | NS |

**Table App 8.** Summary of t-Test.

| Frequency (Hz) | Mix | Temperatures (°C) | | |
|---|---|---|---|---|
| | | 4.4 | 21.1 | 37.8 |
| 25 | CP-A | CNR | CNR | CNR |
| | CP-B | CNR | CNR | CNR |
| 10 | CP-A | CNR | CNR | CNR |
| | CP-B | CNR | CNR | CNR |
| 5 | CP-A | CNR | CNR | CNR |
| | CP-B | CNR | CNR | CNR |
| 1 | CP-A | CNR | CNR | CNR |
| | CP-B | CNR | CNR | CNR |
| 0.5 | CP-A | CNR | CNR | CNR |
| | CP-B | CNR | CNR | CNR |
| 0.1 | CP-A | CNR | CNR | CNR |
| | CP-B | CNR | CNR | CNR |